Volume 11

LLE Review

Quarterly Report

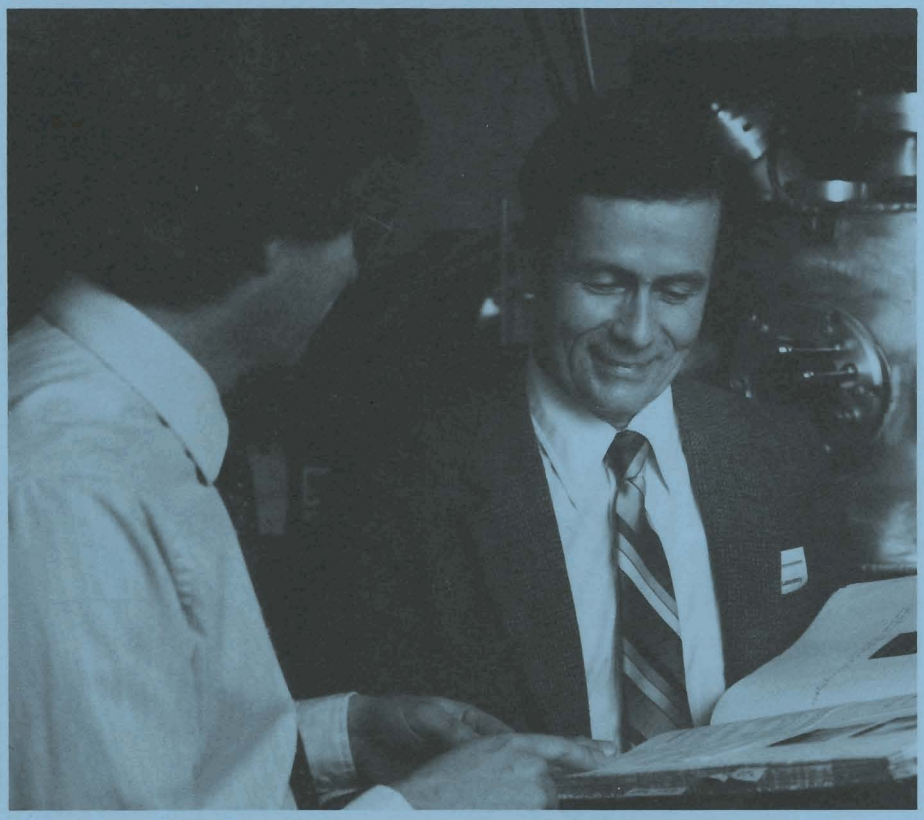

April 1982–June 1982

Laboratory for Laser Energetics
College of Engineering and Applied Science
University of Rochester
250 East River Road
Rochester, New York 14623

Volume 11

LLE Review

Quarterly Report

Editor: J. M. Forsyth
(716-275-5659)

April 1982–June 1982

Laboratory for Laser Energetics
College of Engineering and Applied Science
University of Rochester
250 East River Road
Rochester, New York 14623

CONTENTS

		Page
IN BRIEF		iii
CONTENTS		v
Section 1	LASER SYSTEM REPORT	1
1.A	GDL Facility Report	1
1.B	OMEGA Facility Report	1
Section 2	PROGRESS IN LASER FUSION	3
2.A	Convective-Stimulated Raman-Scattering Instability in UV-Laser Plasmas	3
2.B	Fabrication of Large-Aspect-Ratio, Plastic-Coated, Metal-Shell Targets	8
2.C	Laser Fusion Target Production: Developments in Drill, Fill, and Plug	12
Section 3	DEVELOPMENTS IN PICOSECOND RESEARCH	16
3.A	Applications of the Jitter-Free Signal-Averaging Streak Camera	16
3.B	Subpicosecond Electrical Sampling	22
3.C	High-Repetition-Rate Amplification of Subpicosecond Pulses	29
Section 4	NATIONAL LASER USERS FACILITY NEWS	34
PUBLICATIONS AND CONFERENCE PRESENTATIONS		42

Professor Hans Griem (University of Maryland) is discussing recent experimental results with Tom Bristow (left), the NLUF manager. Professor Griem carried out experiments on the GDL facility which are reported in this issue.

Section 1
LASER SYSTEM REPORT

1.A GDL Facility Report

GDL continued operation as a 0.35 μm irradiation facility during the third quarter of FY82.

A total of 892 shots was delivered by the facility during the period April 1 to June 30, 1982. The shot distribution was as follows:

3ω Target Experiments	71	Shots
X-Ray Program	65	
Damage Test Facility	679	
Alignment	77	
TOTAL	892	Shots

A summary of the experimental work carried out in the 0.35 μm Interaction Physics Program is given elsewhere in this issue.

1.B OMEGA Facility Report

During the third quarter of FY82 a total of 492 shots was fired on the OMEGA laser system. Most of the shots were fired in order to meet the needs of the participants in the National Laser Users Facility program. Most of the month of April was spent in reconfiguring the laser system to produce pulses of 100 ps nominal FWHM. At this pulsewidth, nominal 24-beam energies of 600 joules—with a high of 800 joules and a low of 300 joules—were achieved.

The distribution of OMEGA system shots during the period was:

Target Shots	164
Test Shots	338
TOTAL	502

The breakdown of target shots by primary user was as follows:

University of Illinois	66	Shots
University of Florida	56	
US Naval Research Laboratory	32	
University of Rochester	6	
Diagnostic Tests	4	
TOTAL	164	Shots

Many of the target shots were used by more than one user; this permitted a more rapid calibration and alignment of the experimental instrumentation. A summary of the activities of the users during the period is given elsewhere in this issue.

The latter part of June was spent reconfiguring the facility to produce one nanosecond (nominal) FWHM pulses for the upcoming uniformity and transport experiments. System maintenance was also performed during this period.

Section 2
PROGRESS IN LASER FUSION

2.A Convective-Stimulated Raman-Scattering Instability in UV-Laser Plasmas

It is well known that a number of laser-driven instabilities exist in the corona of laser-produced plasmas.[1] In these instabilities, the incident electro-magnetic (e-m) wave typically decays into a scattered e-m wave of lower frequency and a plasma wave (SRS), or into two-plasma waves ($2\,\omega_p$ decay instability), or into a scattered e-m wave having little or no red shift and an ion-acoustic wave (SBS). All these processes are three-wave processes. Four-wave processes such as self-focusing and modulational instability may also be excited in the corona. The existence of any of these instabilities presents potential problems for laser fusion as they may cause excessive energy loss (SBS), the generation of energetic electrons leading to target preheat (SRS and $2\omega_p$ decay instability), and strong intensity nonuniformities (four-wave processes).

If the existence of some of these instabilities is paired with the necessary theoretical understanding of the processes involved, the experimental signatures of these instabilities may serve as a convenient coronal plasma diagnostic. This is the case with convective SRS which occurs in the underdense corona at $n_e < n_c/4$. In this article, we present some highlights of experiments on SRS backscattering and the theoretical background used to explain the observations. We then apply the theory to obtain time-resolved coronal temperatures from the evolution of the SRS spectra during the laser irradiation interval.

To study SRS backscattering from plane plastic targets, we used the GDL-UV laser facility which delivered up to 50 J in either 0.5 or 1 ns

FWHM pulses at $\lambda = 351$ nm. Intensities on target ranged from 10^{13} to 2×10^{15} W/cm^2. The SRS light backscattered through the lens was extracted from the incident beam path with a dichroic mirror (Fig. 1). This SRS light was then incident on a 1/4 m spectrometer along with a properly timed fiducial derived from the incident beam. The spectrum thus produced was time-resolved with a Hadland 675 ps streak camera with 10 to 20 ps resolution. The work reported here is previously reported work.[2,3]

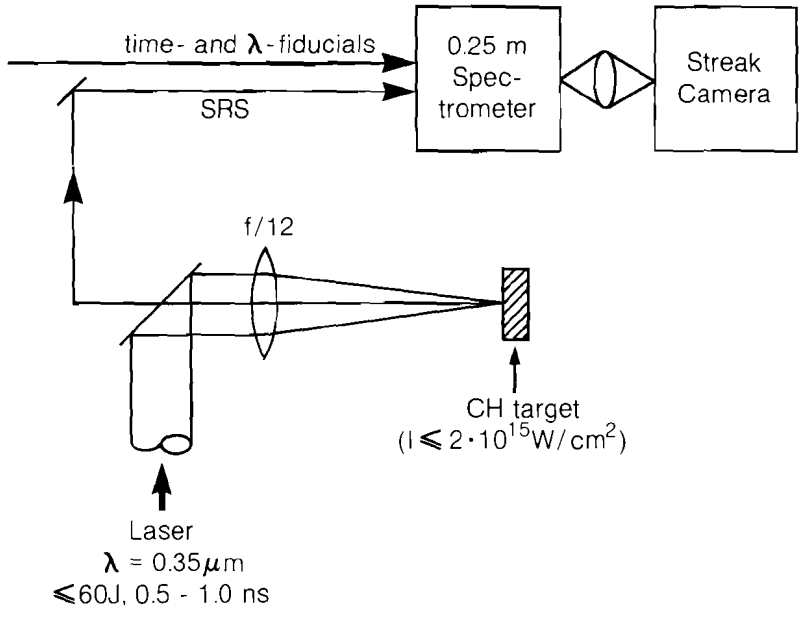

Fig. 1
Experimental set-up for time-resolved SRS backscatter spectra.

A typical time-resolved spectrum is shown in Fig. 2 for a 0.5 ns pulse at 10^{15} W/cm^2 on target. Three distinct components are seen in these spectra: (a) a component due to convective SRS around 450 to 550 nm, (b) $\omega/2$ radiation due to reradiation from the 2 ω_p decay instability at 720 nm, and (c) the delayed incident laser fiducial at 720 nm (second order of fundamental), used for timing and for calibration of wavelength.

In this report, we will concentrate on the interpretation of the SRS signal. This radiation originates in the corona at densities $0.01 < n_e/n_c < 0.2$. Figure 3 schematically depicts the plasma corona with the incident laser penetrating into the dense plasma up to n_c. In the region where convective SRS occurs, the incident e-m wave may decay into a scattered e-m wave and an electron plasma wave, both obeying the energy and momentum conservation laws as well as the relevant dispersion relations (Fig. 3). The corresponding vector diagram is shown in the insert. We note that due to the weak scaling of the frequency of the plasma waves with k_p, we obtain essentially monochromatic, isotropically scattered light at any particular plasma density.

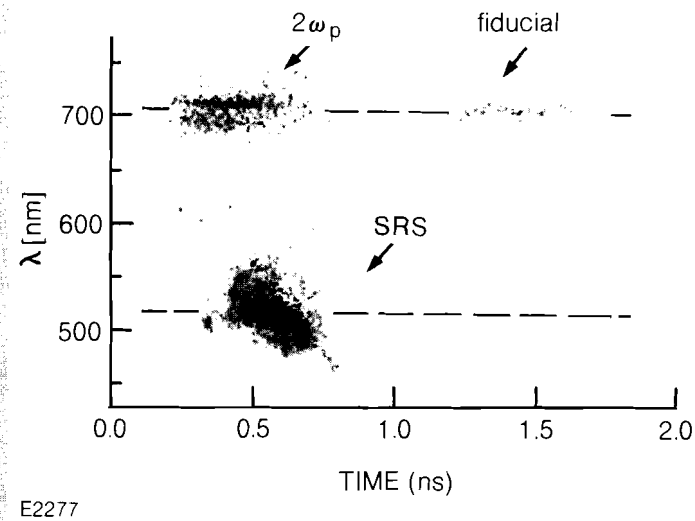

Fig. 2
Typical time-resolved SRS spectrum obtained from plastic (CH) targets at 10^{15} W/cm². The different features are due to convective SRS (450-550 nm), re-radiation from the $2\omega_p$ decay instability (double line at 720 nm), and a timing and wavelength fiducial derived from the incident beam (2 x 351 nm).

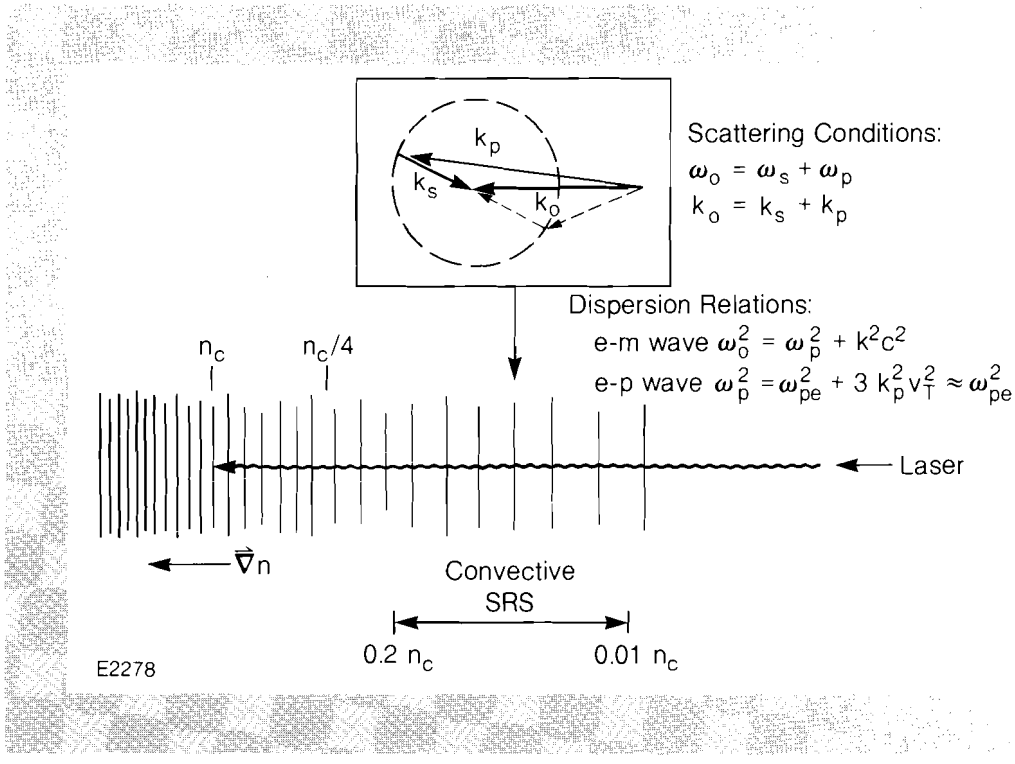

Fig. 3
Schematic diagram of the plasma corona showing typical regions over which SRS is observed. The inset shows a representative k vector diagram for the parametric SRS process. The governing laws for the conservation of energy and momentum and the relevant dispersion relations are also indicated.

However, the scattered light frequency is quite sensitive to the density at which the scattering occurs since $\omega_p \approx \omega_{pe} \propto \sqrt{n_e}$ and $\omega_s = \omega_o - \omega_p \approx \omega_o[(n_e/n_c)^2]$. This results in $\omega_o/2 < \omega_s < \omega_o$. Here the symbols ω_o, ω_s, ω_p, ω_{pe}, are the angular frequencies, respectively, of the incident and scattered e-m waves, the electron plasma wave, and the electron plasma frequency. The electron density is denoted by n_e, and n_c is the critical density at which $\omega_{pe} = \omega_o$. (For typical

coronal temperatures of 1 to 3 keV the thermal correction factor in the dispersion relation for the plasma waves is very small.)

The SRS intensity observed depends on a number of factors: the thermal e-m noise level, the SRS gain coefficient, and the incident light intensity, through

$$I_{SRS} = I_{noise} e^{2\pi G_{SRS} I_L}, \quad (1)$$

where I_{SRS}, I_{noise}, I_L, are, respectively, the SRS, thermal e-m noise, and incident laser intensities. G_{SRS} is the convective SRS gain factor. The threshold intensity for this process, I_{th}, is traditionally[1] defined by $G_{SRS} \cdot I_{th} = 1$. The thermal e-m noise intensity is strongly frequency-dependent and is obtained by correcting the plasma black body spectrum for the optical depth between the density at which the SRS takes place, and the critical density at the frequency of interest. In Fig. 4 we have plotted the wavelength-dependent e-m noise intensity along with typical SRS gain factors. The latter show a short-wavelength cut-off which strongly depends on the coronal electron temperature and is due to electron Landau damping of the plasma wave generated in the SRS process. These gain factors were recently obtained by E. A. Williams[4] by analyzing the existing homogeneous theory of SRS and extending it to inhomogeneous plasmas.

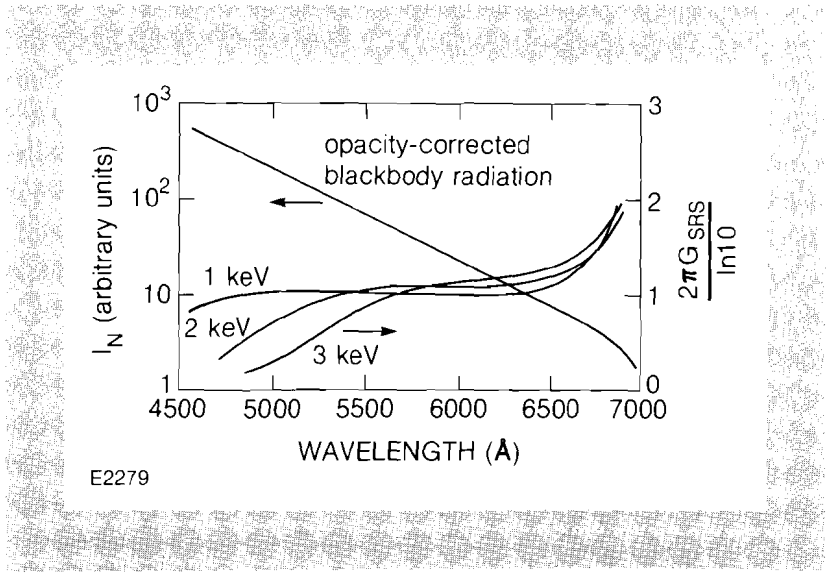

Fig. 4
Wavelength dependence of the e-m noise intensity from which the convective SRS grows, along with calculated[4] SRS gain coefficients. The short-wavelength cut-off is due to electron Landau damping.

Folding the gain factors and the e-m noise intensities according to Eq. (1), one obtains SRS spectra for different temperatures as shown in Fig. 5. These spectra generally exhibit a strongly temperature-dependent short-wavelength cut-off due to the corresponding behavior of the SRS gain coefficient. Close to threshold these spectra also exhibit rather narrow (20-70 nm) distributions whose peaks shift to longer wavelength as the temperature increases. By plotting the wavelengths of the peaks of the calculated spectra as a function of the coronal electron temperature, one obtains the curve shown in Fig. 6. Thus, by estimating the time-dependent wavelengths of the peaks of the experimental spectrum in Fig. 2, one can estimate the coronal temperature evolution during the laser pulse. The range of experimental temperatures thus obtained is

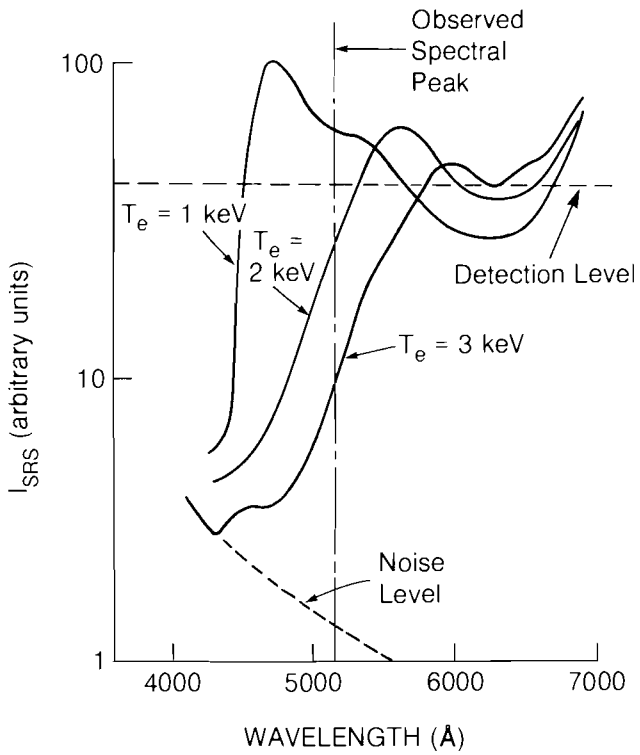

Fig. 5
Calculated SRS spectra near threshold. The strong temperature dependence of the peaks is clearly evident.

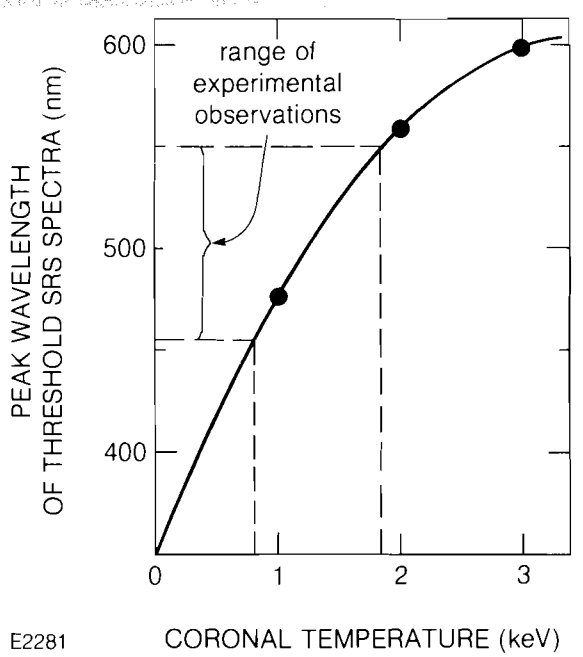

Fig. 6
Temperature dependence of the short-wavelength peaks of the SRS spectra near threshold. Also indicated are the maximum wavelengths observed experimentally for these peaks for 0.5 and 1 ns irradiation. In addition, typical ranges are shown for the coronal temperatures deduced from the experiments.

shown in Fig. 6 for both 0.5 and 1 ns irradiation. The on-target intensities were 10^{15} and 5×10^{14} W/cm^2, respectively. The deduced temperatures (0.8 to 1.8 keV) correspond very closely to those calculated with 1-D and 2-D hydro-codes such as LLE's *LILAC* and *SAGE*.

Using Figs. 2 and 6, we have deduced the time-dependent electron temperature in the corona (Fig. 7). Both the temporal behavior and the absolute values of the coronal temperatures track the hydro-code calculations quite well; however, independent coronal temperature measurements are required in order to accept the present technique as a viable coronal temperature diagnostic. Nevertheless, the great potential inherent in the SRS spectra as a coronal temperature diagnostic is demonstrated here for the first time.

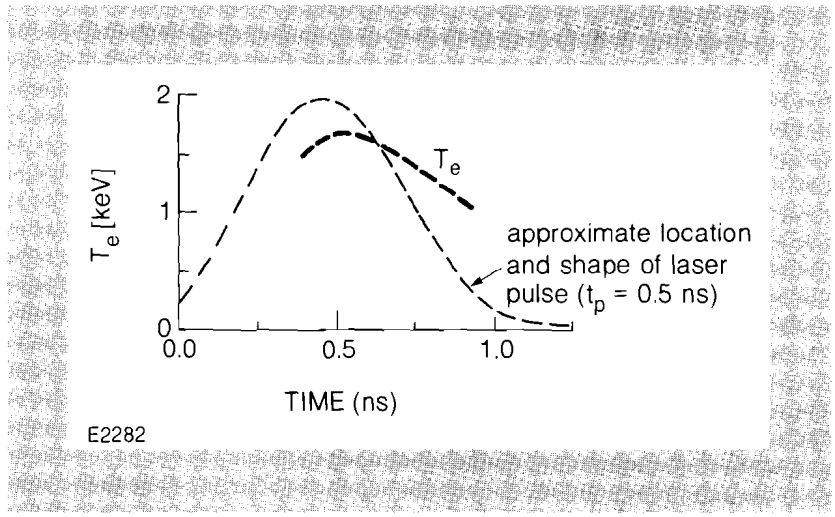

Fig. 7
Time-dependent coronal temperatures deduced from Figs. 2 and 6. The approximate location of the incident laser pulse is also shown.

REFERENCES
1. M. N. Rosenbluth, *Phys. Rev. Lett.* **29**, 565 (1972); C. S. Liu, in *Advances in Plasma Physics*, edited by A. Simon and W. B. Thompson (Wiley, New York, 1976), Vol. 6, p. 121.
2. K. Tanaka, L. M. Goldman, W. Seka, M. C. Richardson, J. M. Soures, and E. A. Williams, *Phys. Rev. Lett.* **48**, 1179 (1982).
3. K. Tanaka, Ph.D. thesis, University of Rochester, Laboratory for Laser Energetics, 1982.
4. E. A. Williams (private communication).

2.B Fabrication of Large-Aspect-Ratio, Plastic-Coated, Metal-Shell Targets

A new mandrel material has been found for making large-aspect-ratio, plastic-coated, metal-shell diagnostic targets using the leachable mandral technique. A typical diagnostic target, shown in Fig. 8, has a diameter of 400 μm and material thicknesses of metal and hydrocarbon that are, respectively, 0.3 μm and 3 μm. The diagnostic targets are intended for use as an x-ray source in backlighting experiments[1] or for studying uniformity of implosion. The main difference between this target and

typical inertial fusion targets is that this target does not contain a glass microballoon. This required a substantial modification of the usual target fabrication technology.

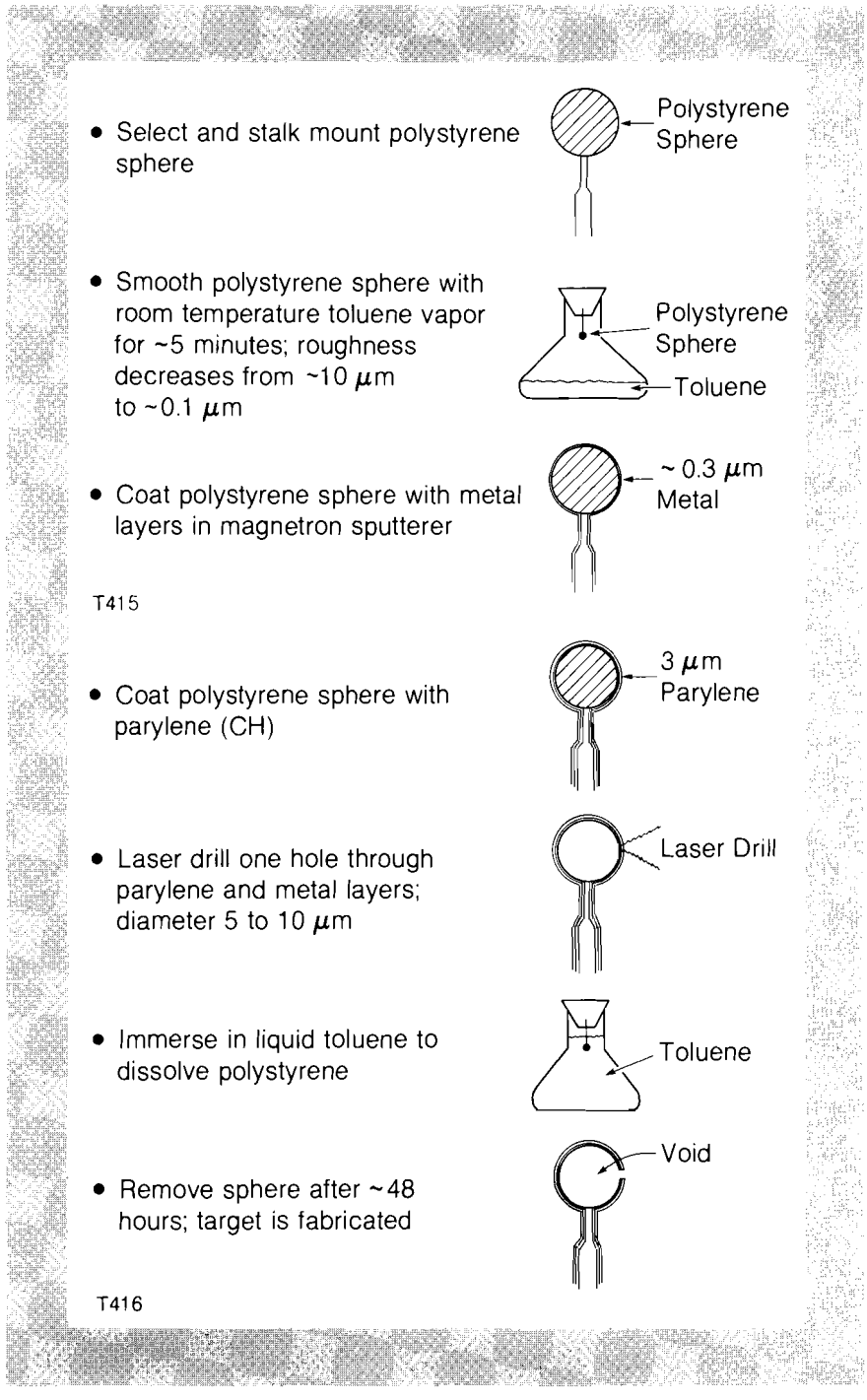

Fig. 8
Sequence for fabricating large-aspect-ratio, plastic-coated, metal-shell diagnostic targets.

A number of different approaches have previously been investigated for the fabrication of such a diagnostic target. These include the hemispherical shell approach,[2] the leachable metal mandrel process,[3] and the coating of a prefabricated metal shell.[4] In the hemispherical shell method, two hemispherical shells are first produced by any one of various methods. Then these half-shells are carefully mated and bonded.

Because of the mechanical handling during this process, the shell walls must be relatively thick. Furthermore, the positioning and bonding process inevitably produces seams and leaves deposits of bonding adhesives. This approach is very time-consuming and requires a highly skilled operator.

In the leachable metal mandrel process, a metal mandrel such as a copper ballbearing is overcoated with a thin metal layer. The copper is then leached through a drilled hole in the coating by a strong acid, leaving a free-standing metal shell. The acid leaching step limits the types of metal shells that can be formed. Paraffin has also been used as the leachable mandrel material to circumvent the acid leaching step.[5] This, however, presents problems during the metal-coating step because paraffin has a low melting temperature. Paraffin mandrel sphericity is also difficult to maintain during the process. Prefabricated, hollow metal shells would simplify the fabrication process by eliminating the entire leaching step. Unfortunately, metal shells currently available are of poor quality, are too thick-walled, and are available in only a single material, a nickel alloy. This necessitated the investigation of more suitable materials for mandrels.

The desired mandrel should be: (1) highly spherical and smooth, (2) easy to coat with various metals while maintaining mandrel sphericity or surface smoothness, (3) selectively leachable through a small hole without damage to the thin metal coating. Spheres of a glassy polymer that are easily soluble at room temperature would meet these requirements. We have successfully developed a fabrication procedure for making the desired high-aspect-ratio, plastic-coated, metal-shell diagnostic targets based on the polymer mandrel.

Figure 8 illustrates the fabrication steps. The sequence begins with a selection of a polystyrene sphere of a proper size and then mounting the sphere on a stalk. The surface finish of commercially available polystyrene spheres is not acceptable but this can be smoothed by exposure to toluene vapor for 5 minutes. This reduces the surface features from approximately 10 μm in height to less than 0.1 μm. A longer exposure deforms the spherical mandrel. The smoothed polystyrene sphere is next coated with the required metal by using magnetron sputtering. This metal-sputter coating should be performed at temperatures below the glass transition temperature of polystyrene, 90°C, or else the polystyrene mandrel will be deformed. After coating parylene over the metal layer, a hole of 5~10 μm diameter is drilled through the coatings by multiple laser pulses from the Diagnostic Evaluation Laser (DEL). The entire assembly is then immersed in toluene for 48 hours during which period the polystyrene mandrel is dissolved and leached out through the hole. Removal of the assembly from the toluene leaching bath leaves a finished diagnostic target.

In this procedure, the surface smoothing step is important because the metal coating replicates the surface texture of the mandrel. Figure 9 shows the surface of the mandrel prior to and after exposure to the solvent vapor. The characterization of the diagnostic target fabricated by this procedure was carried out with an optical microscope. For this in-

(a)

(b)

Fig. 9
Surface smoothing of the polystyrene mandrel by solvent vapor.
a) mandrel surface prior to exposure
b) surface after exposure to toluene for 5 minutes.

vestigation, the metal layer was not coated, and a plastic shell was prepared by the procedure detailed in Fig. 8. Figure 10 is an interferogram of the plastic shell and shows the uniform wall thickness produced by this process.

Diagnostic targets having a diameter of approximately 50 μm have been fabricated by this process with metal layers of copper, titanium, and aluminum. Other metals are not expected to present unusual difficulties. Metal layers are usually a fraction of a micrometer thick, typically 0.3 μm, but much thinner layers can also be coated.

The developed procedure is now routinely used to fabricate laser fusion diagnostic targets.

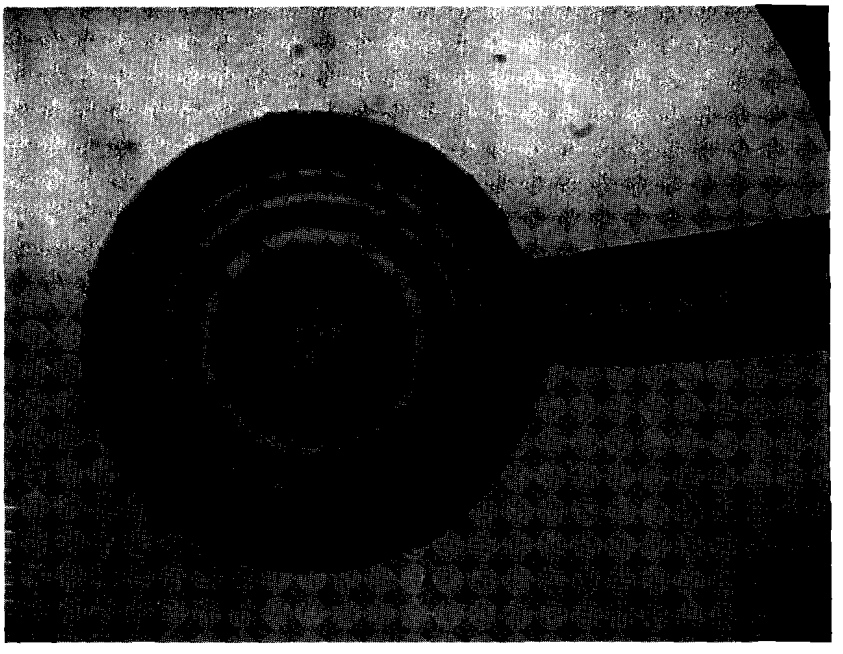

Fig. 10
Optical interferogram of parylene shell fabricated by the present procedure.

REFERENCES
1. V. Rupert, D. Matthews, H. Ahlstrom, D. Attwood, R. Price, L. Coleman, K. Manes, and V. Slivinsky, *LLNL Report* UCRL-86424 (1981).
2. C. W. Hatcher, L. E. Loreusen, and B. W. Weinstein, *J. Vac. Sci. Technol.* **18**, 1187 (1981).
3. K. W. Bieg and J. Chang, Topical Meeting on ICF, 26-28 February 1980, paper THB 20; W. J. McCreary, D. B. Court, G. Simonsic, J. Bucheui, and D. S. Catlett, *ibid.* paper THB 25.
4. J. M. Kendall, M. C. Lee, and T. G. Wang, *J. Vac. Sci. Technol.* **20**, 1091 (1982).
5. T. Norimatsu, H. Axechi, M. Yoshida, R. Ohashi, and C. Yamanaka, Topical Meeting on ICF, 26-28 February 1980, paper WCI.

2.C Laser Fusion Target Production: Developments in Drill, Fill, and Plug

Laser fusion target designs frequently require glass microballoons (GMB's) filled with non-fuel diagnostic gases. These "diagnostic" targets are necessary for measuring target temperature, density, hydrodynamic stability, and for calibration of the diagnostic equipment used to measure these parameters during target implosion experiments. Helium and neon are two diagnostic gases that can be permeated through the GMB wall simultaneously with the deuterium-tritium fuel gas. Other diagnostic gases such as argon, krypton, and xenon cannot be easily permeated, since they require excessively high temperatures and exhibit very long permeation times.

The method for making non-fuel diagnostic targets that we have successfully put into production is referred to as the "Drill-Fill-Plug" technique.[1-4] The fabrication procedure involves laser-drilling a hole through the GMB wall, placing a piece of glass-plug-forming material over the hole, filling the GMB with gas in a pressure chamber, then heating the assembly to melt the plug, thus sealing the gas inside the GMB.

The fabrication process begins with selecting GMB's of the proper diameter, wall thickness, and uniformity. These are then fastened to a 4 mm x 25 mm chromium-coated glass slide using sodium chloride crystals as a bonding material. Typically, ten GMB's are put on one glass slide, and the quantity of sodium chloride used must be tailored to the size of the GMB's.

A nominal 1 μm diameter hole is then drilled through the wall of each GMB using a 1.054 μm wavelength yttrium lithium fluoride (YLiF) laser. A typical hole is shown in Fig. 11. This is drilled using the Diagnostic Evaluation Laser (DEL) system with a full-pulse train that consists of approximately 15 pulses of 80-100 ps duration delivered over a period of approximately 1 μs.

Glass-plug material is formed by blowing a bubble of molten Corning #7570 solder glass until it ruptures. A piece of the bubble is selected for

Fig. 11
Scanning electron micrograph of a laser-drilled hole in a glass microballoon which is mounted on sodium chloride crystals.

wall thickness, typically 1-2 μm, using an interferometer. The lateral dimensions of the selected piece are always much greater than required to form a plug, so the selected piece must be chopped up into hundreds of fragments. These fragments are then placed on the bottom of a cover slip mounted under a high-power microscope where a single fragment with the desired lateral dimensions, 5-10 μm, is selected. A photograph of these fragments is presented in Fig. 12.

T470

Fig. 12
1280x photomicrograph of solder glass which was blown into a bubble, and then crushed to make thin sheet plugs.

The drilled GMB's are placed on the stage of the microscope where each hole is aligned with a selected glass plug and then raised to bring the hole into contact with the plug. With careful manipulation, the glass plug material sticks to the top of the GMB and remains there through the rest of the process.[4]

The glass slide holding the GMB's is then placed in a small chamber

that is evacuated and then backfilled with the proper pressure of specified gases. A Nichrome wire coiled around the GMB's is used to locally heat and melt the glass-plug material over the hole. This heating cycle lasts about 4 minutes. The heater power must be carefully adjusted to the proper level for each gas mixture and pressure. An example of a large plug melted onto a GMB is shown in Fig. 13.

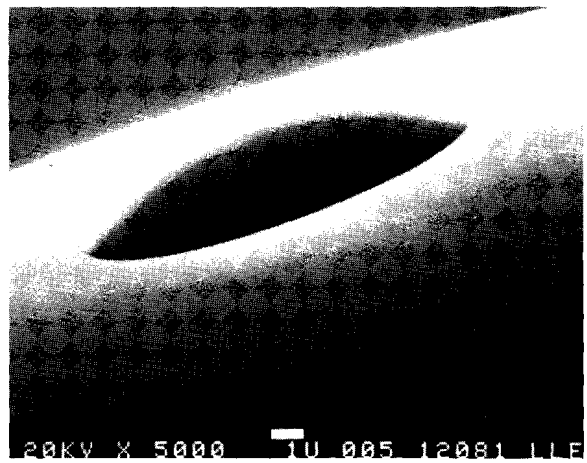

Fused plugs are typically 10 μm in diameter and 1 μm high

- Gas retention - no measurable loss from 10 atm Ar-filled shells after 36 days at STP
- Fill pressure - greater than 60 atm for shells with diameter/wall = 100
- Fuel permeation - hydrogen isotopes can be permeated without plug damage

T440

Fig. 13
Scanning electron micrograph of a large plug, 14 μm in diameter, melted onto the wall of a glass microballoon.

After removal from the plugging chamber, the plugged and filled GMB's can be mounted for additional process steps, such as coating, or sent to be filled with the permeable fuel gas. The fuel permeation is performed at 350°C, which is 100°C less than the softening temperature of the plug glass.

Over 240 GMB's have been successfully filled with non-permeable gases using the Drill-Fill-Plug process. Pressures were from 2 to 60 atm, using argon, neon, and krypton, and with mixtures of neon and argon. Twenty atm of DT have been permeated into GMB's filled and plugged with 2 atm of argon. The overall fabrication process yield has been about 66%. However, when GMB's of a single diameter and wall thickness are used for a series of runs using the same fill specifications, the yield improves with each slide of GMB's and approaches 100%. When the target specifications are changed, the yield drops substantially, but increases as all the parameters are optimized for the new target design.

One important change that is planned for the Drill-Fill-Plug apparatus setup is a complete replumbing of the gas handling tubing. This will re-

duce the dead volume by a factor of 10 and reduce consumption of the rare diagnostic gases.

ACKNOWLEDGMENTS

The author wishes to thank Alain Coudeville, Centre d'Etudes de Limeil, for suggesting the plug glass bubble-blowing technique and S. Butler, Rochester Institute of Technology, for the plugging chamber development and solder glass selection. We also thank J. Dunsmuir of Exxon Research & Development for personally teaching us the plug placement technique.

REFERENCES

1. S. Butler and B. Cranfill, *Technical Digest of Topical Meetings on Inertial Confinement Fusion* (Optical Society of America, Washington, D.C., 1980), paper THB10.
2. H. W. Deckman, J. Dunsmuir, G. M. Halpern, and J. Drumheller, *Technical Digest of Topical Meetings on Inertial Confinement Fusion* (Optical Society of America, Washington, D.C., 1980), paper TUE3.
3. S. M. Butler and M. H. Thomas, *J. Vac. Sci. Technol.* **18**, 1291 (1981).
4. H. W. Deckman, J. H. Dunsmuir, G. M. Halpern, and J. P. Drumheller, *J. Vac. Sci. Technol.* **18**, 1258 (1981).

Section 3
DEVELOPMENTS IN PICOSECOND RESEARCH

3.A Applications of the Jitter-Free Signal-Averaging Streak Camera

Introduction

The picosecond streak camera is an extremely versatile instrument for the detection of fluorescence. The photocathode element responds over a wide spectral range (~200 nm to 800 nm for S-20 response), it responds equally to either polarization of incident light, and it is not selective in terms of solid angle of incoming light. This degree of versatility is not matched by other methods of fluorescence detection with a few picosecond resolution such as the optical Kerr shutter,[1] or fluorescence upconversion.[2] These other techniques are, however, jitter-free.

We recently demonstrated a nearly jitter-free (2 ps) operation of a streak camera[3-6] using various high-power picosecond photoconductors. Since this first demonstration, we have proceeded to apply this system to a wide range of studies in solid-state physics, biophysics, and chemistry. We discuss here several recent results in these areas which illustrate the importance of signal averaging in picosecond fluorescence kinetics experiments.

Streak Camera

The jitter-free streak camera in its present form[5] (Fig. 14) uses a high-power picosecond photoconductive switch made of chromium-doped GaAs, a semi-insulating material.[7] When excited by a single laser pulse from an active-passive mode-locked Nd:YAG laser, the switch starts conducting and charges the deflection plate of a Photochron-II streak camera tube. A portion of the same optical pulse is frequency-doubled,

and used to excite a sample. Fluorescence is collected and imaged onto the photocathode through bandpass or cutoff filters. The streaked image is amplified in a four-stage magnetically-focused intensifier stage, and recorded with an optical multichannel analyzer image device (Princeton Applied Research Model OMA II).

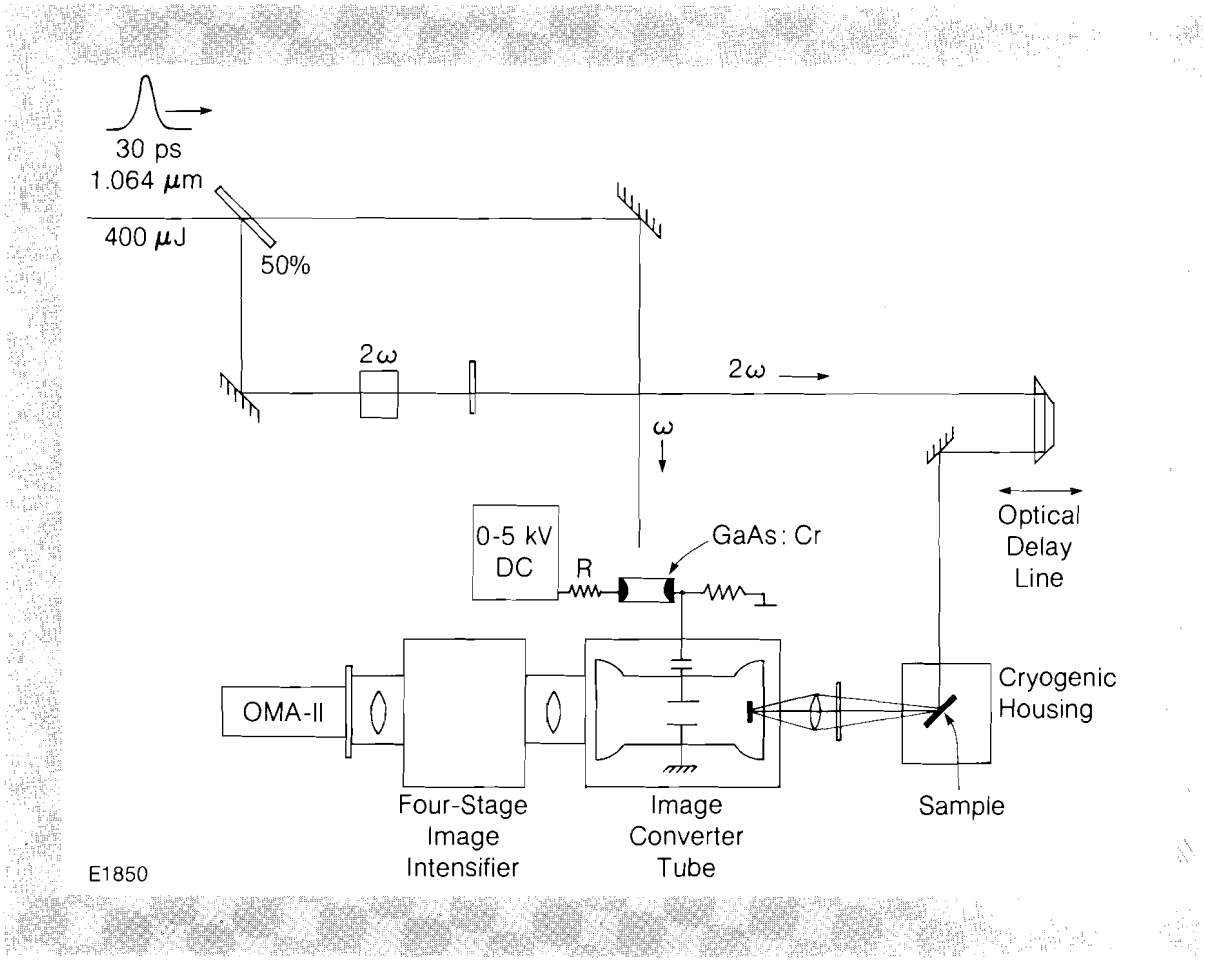

Fig. 14
Experimental configuration. A single pulse from an active-passive mode-locked Nd:YAG oscillator is directed upon a high-power picosecond semiconductor switch. The deflection plate is charged in ~1 ns in synchronization with the excitation pulse for the sample under study. The sweep speed is linearly proportional to the DC bias voltage applied to the switch.

The sweep speed is linearly proportional to the bias voltage applied to the switch, and there is no inherent time delay in the switching process. Sweep speeds of between 6 ps/mm and 50 ps/mm are obtained in this way.

In order to obtain 2 ps jitter, it is necessary for the laser system to satisfy several criteria: energy stability ± 15%, energy contrast ~ 10^5, and pulsewidth stability ± 5%. These are easily obtainable on a routine basis with an active-passive mode-locked laser,[8] but not with a passively mode-locked laser.

Since the switch operates in a linear photoconductive mode as opposed to an avalanche mode, it has a very long lifetime. We have used one switch for two years now, with no apparent deterioration.

We have also applied this technique to several other types of streak cameras with success: Electro-Photonics, Hadland, Thomson-CSF, and GEAR.[9]

Applications

Many luminescence phenomena in the area of solid-state physics exhibit decay times of up to several hundred microseconds. In the case of luminescence from amorphous semiconductors, decay times vary from nanoseconds to milliseconds. We have made the first measurement of luminescence from an amorphous semiconductor on the picosecond time scale in amorphous As_2S_3[10,11] (Fig. 15). In this experiment, the picosecond signal was extremely weak, such that a single shot at the highest detection system gain (10^7) was a statistical distribution of photoelectron events. After averaging up to 300 shots, it was possible to obtain a characteristic decay time (see insert). A strong temperature dependence of the decay rate was found by repeating this measurement at various temperatures. The interpretation of this data is given in detail in Ref. 11. In temperature cycling experiments, long-term stability is critical due to the slow thermal response time of sample holders.

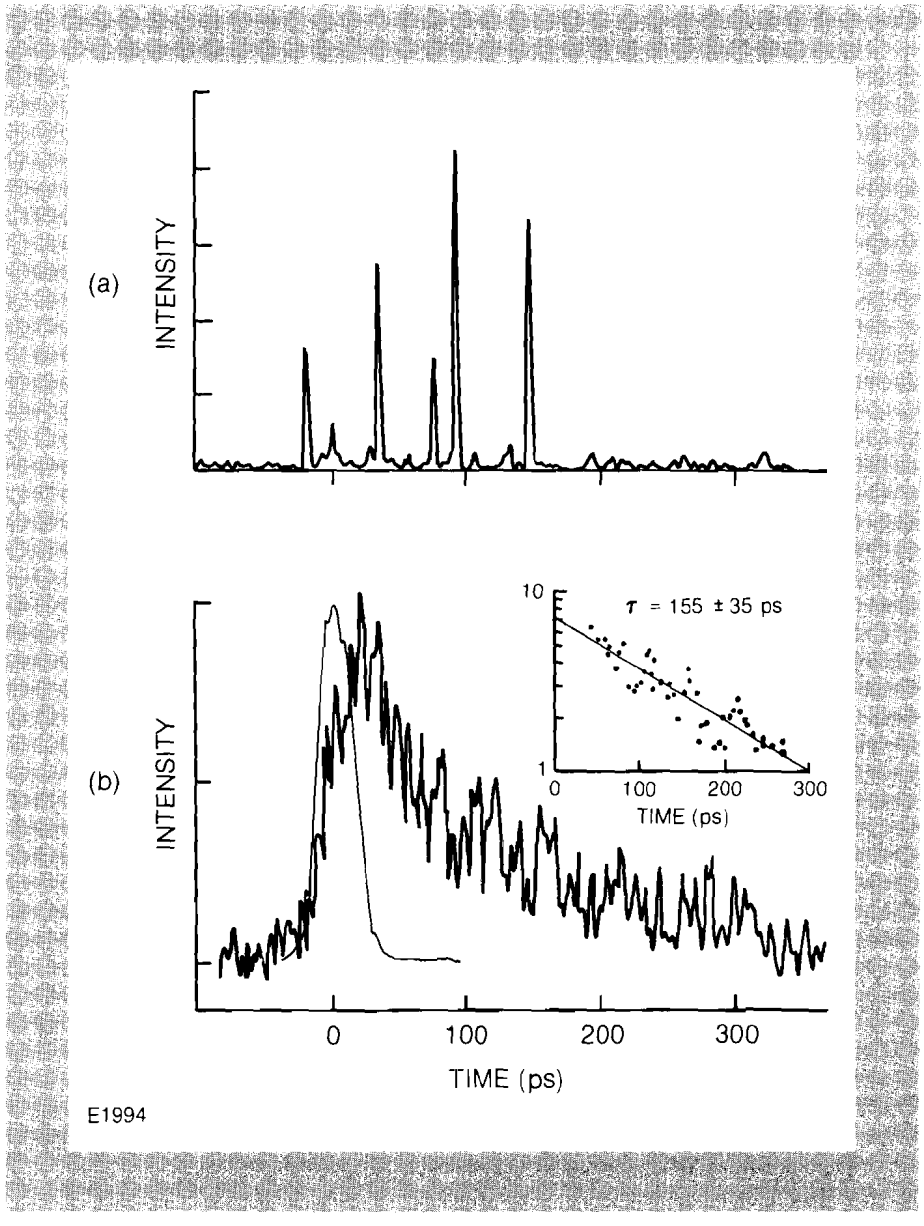

Fig. 15
Averaging of very weak signals. Shown are (a) one and (b) 300 shots of luminescence of amorphous As_2S_3 under excitation by a 30 μJ pulse at 532 nm. Despite the extremely weak signal, signal-averaging allows a determination of the decay time (inset). Also shown are 30 shots of the scattered excitation pulse at t = 0.

In other studies in this area, we have investigated fluorescence kinetics of cis- and trans-polyacetylene,[12] and vibrational relaxation of molecular ions, color centers and heavy metal ions in alkali-halide crystals.[13]

We have measured the fluorescence kinetics of biosystems at relatively high excitation levels ($\sim 10^{18}$ photons/cm^2) in order to study the process of exciton annihilation. In a recent experiment,[14] we have measured the fluorescence of Photosystem-I[15] particles under excitation by the second harmonic (532 nm) pulse (Fig. 16) from a Nd^{+3}:YAG laser. We have obtained a good analytical fit to the data assuming a simple bimolecular recombination rate. The calculated curve is the solution to:

$$\dot{N} = -\frac{N}{\tau} - \gamma N^2 + \sigma I N_o \qquad (2)$$

where N is the number density of excited species, τ is the ordinary decay time, γ is the bimolecular recombination constant, σ is the absorption cross section, I is the pump intensity, and N_o is the ground state density, assumed constant. This fit suggests that a simple biomolecular recombination kinetic model is appropriate in this complex system over a large intensity range. By averaging 100 shots we obtained a sufficiently high signal-to-noise ratio to make a determination of γ to within $\pm$ 10%. The value of γ in a system is related to the topology and accurate

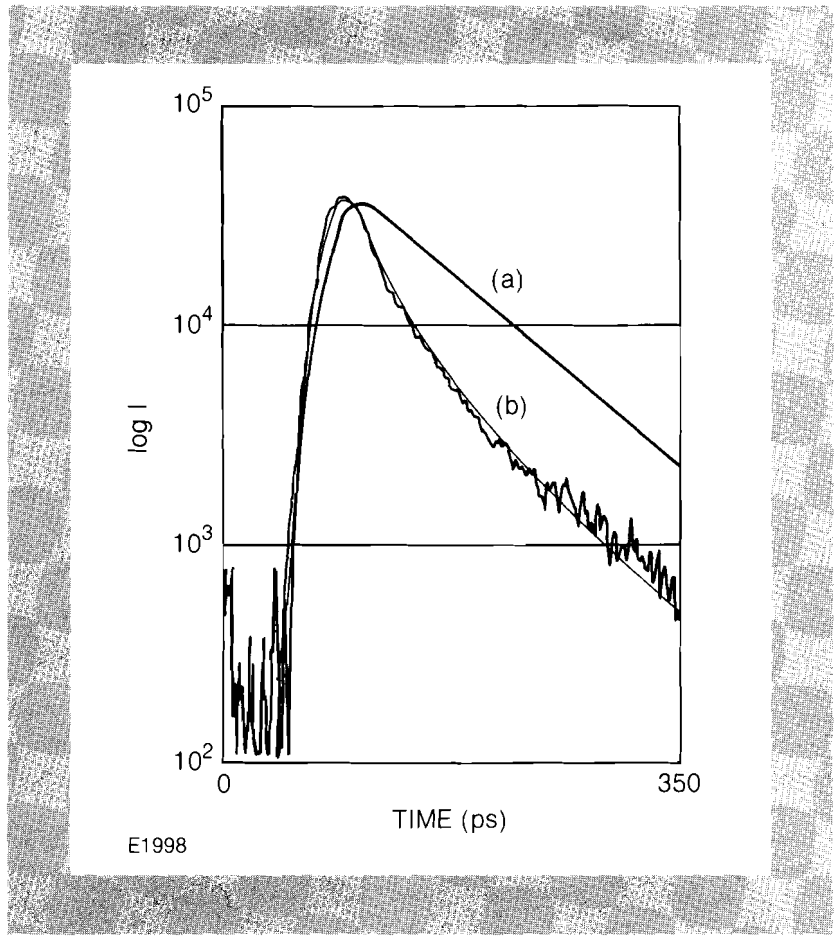

Fig. 16
Detailed curve fitting. Fluorescence of Photosystem-I particles under excitation at 532 nm. 100 shots of fluorescence are accumulated.
a) the solution to Eq. (2) asuming $\gamma = 0$ and $\tau = 80$ ps (the fluorescence decay time
b) the solution to Eq. (2) assuming a simple bimolecular recombination
The fit is extremely sensitive to the value of γ used, and its value can be determined to within 10% by this method.

measurements of γ in many systems may provide additional insight into the role of excitons in biological systems.

In other applications in biophysics, we have made measurements of the excitation intensity dependence of chlorophyll a/b protein fluorescence,[16] anisotropy decay time constants of Tryptophan in various environments,[17] the temperature dependence of purple membrane fluorescence lifetime,[18] the energy transfer rate in spinach chloroplasts,[19] and the fluorescence decay of hematoporphyrin derivative.[20]

The jitter-free streak camera, coupled to the OMA-II—which has the capability to do multi-track scanning—is a powerful tool to probe depolarization of fluorescence. Depolarization is measured experimentally by measuring the intensities of fluorescent components, $I_{\perp}(t)$ and $I_{||}(t)$, polarized perpendicular to and parallel to the excitation polarization, respectively. The ratio of these components formed by

$$R(t) = \frac{I_{||} - I_{\perp}}{I_{||} + 2I_{\perp}} \tag{3}$$

is of interest and is very sensitive to noise in the component signals. In Fig. 17, we show one result of measurement of fluorescence depolarization of Rhodamine-6G in water.[21] An average of 50 shots were fired in order to obtain an adequate signal-to-noise ratio for a detailed study of the dependence of the decay time as a function of solvent viscosity and ionic strength.[21] Data for $I_{\perp}$ and $I_{||}$ were simultaneously accumulated in separate files. In some cases, we averaged signals from up to 200 shots in order to measure the decay constant to within 5%. Decay times as short as 10 ps may be measured with this technique.

In other applications, we have measured fluorescence decay of Phthalazine in various solvents[22] and fluorescence kinetics of molecular monolayers on solid surfaces.

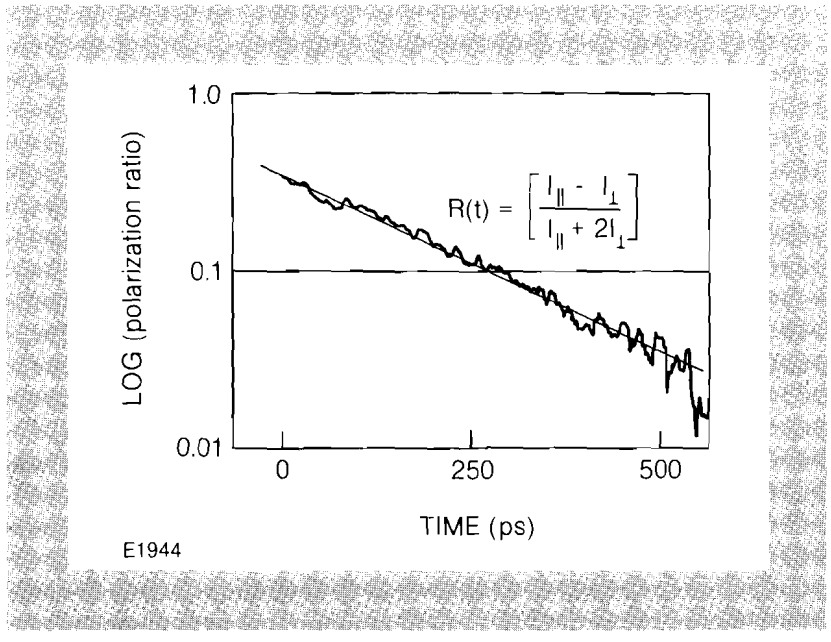

Fig. 17
Measurement of fluorescence depolarization. Fluorescence anisotropy decay of Rhodamine-6G in water. The anisotropy parameter R(t) is calculated from 50 shot averages of $I_{\perp}$ and $I_{||}$. The high signal-to-noise ratio of these data allow for a determination of the value of the anisotropy decay time to within 5%. Decay times as short as 10 ps can be measured with this method.

Conclusion

The signal-averaging capability of the jitter-free streak camera makes it a powerful diagnostic in picosecond fluorescence kinetics experiments. By averaging 50 shots, one has access to ± 0.5 ps timing stability.[5,13] The system is capable of performing both high-power excitation experiments ($\sim$GW/cm^2) and low-excitation intensity experiments (10^{12} photons/cm^2). In the case of long fluorescence lifetimes, high sensitivity is needed to record picosecond time-scale information. The high stability of the system makes possible extended studies where only one parameter is changed, such as temperature, excitation intensity, collection wavelength, or detector polarization.

The use of the DC-biased photoconductive switch operated at room temperature results in a simple system to operate which avoids the timing drift and inherent jitter which are characteristic of other sweep driver systems. This permits the simple accumulation of many successive (laser-initiated) events resulting in a dramatic increase in the precision of measurement. With the versatility of the streak camera coupled to the jitter-free feature, one has a powerful diagnostic for picosecond fluorescence kinetics studies.

REFERENCES

1. M. A. Duguay and J. W. Hansen, *Appl. Phys. Lett.* **15**, 192 (1969).
2. B. Kopainsky and W. Kaiser, *Opt. Commun.* **26**, 219 (1978).
3. G. Mourou and W. Knox, *Appl. Phys. Lett.* **36**, 623 (1980).
4. M. Stavola, G. Mourou, and W. Knox, *Opt. Commun.* **34**, 404 (1980).
5. W. Knox and G. Mourou, *Opt. Commun.* **37**, 203 (1981).
6. G. Mourou, W. Knox, and S. Williamson, "Picosecond High-Power Switching and Applications," *Laser Focus*, April 1982, p. 97.
7. C. H. Lee, *Appl. Phys. Lett.* **20**, 84 (1977); G. Mourou and W. Knox, *Appl. Phys. Lett.* **35**, 492 (1979).
8. W. Seka and J. Bunkenburg, *J. Appl. Phys.* **49**, 2277 (1978).
9. W. Knox, "Picosecond High-Power Switching at the Los Alamos National Laboratory," *LASL Report* LA-8720.
10. T. Orlowski, B. Weinstein, G. Mourou, W. Knox, and T. M. Nordlund, "Picosecond Radiative Recombination in Amorphous As_2S_3," APS Meeting, Dallas, Texas, March 1982.
11. T. Orlowski, B. Weinstein, W. Knox, T. M. Nordlund, and G. Mourou, *Phys. Rev. B* **26**, 4777 (1982).
12. J. Andrews, W. Knox, and B. Wittmershaus, to be submitted to *Chemical Physics Letters*.
13. W. Knox, Ph.D. thesis, University of Rochester (to be published).
14. B. Wittmershaus and C. Huang, "Time-Dependence of the Fluorescent Emission of Detergent-Free Photosystem-I Particles," Tenth American Society of Photobiology Conference, Vancouver, B.C., June 1982.

15. C. Huang and D. S. Berns, submitted to *Archives of Biochemistry and Biophysics*.

16. T. M. Nordlund and W. Knox, "Lifetime of Fluorescence from Chlorophyl a/b Proteins: Excitation Intensity Dependence," *Biophys. J.* **36**, 193 (1981).

17. T. M. Nordlund and D. Podolski, "Subnanosecond Fluorescence Measurements of Tryptophan and Tyrosine Motions," Tenth American Society of Photobiology Conference, Vancouver, B.C., June 1982.

18. R. Frankel, W. Knox, A. Lewis, G. Mourou, T. M. Nordlund, and G. Perrault, "Temperature-Dependence of Purple Membrane Fluorescence Lifetime" (to be published).

19. J. Breton, N. Geacintov, R. S. Knox, W. Knox, T. M. Nordlund, J. Waldmeyer, and B. Wittmershaus, "Energy Transfer Kinetics of Spinach Chloroplasts" (to be published).

20. C. Hanzlik, T. M. Nordlund, and W. Knox (to be published).

21. D. Podolski, Ph.D. thesis, University of Rochester (to be published).

22. R. W. Anderson and W. Knox, "Time-Resolved Fluorescence Decay Measurements in Phthalazine," *J. Lumin.*, **24/25**, 647 (1981).

3.B Subpicosecond Electrical Sampling

The availability of picosecond and subpicosecond laser pulses has made possible the investigation of material processes in the subpicosecond time range. For the most part, to date, these studies have been of an optical nature. With the advent of picosecond photodetectors,[1-7] photoconductor switches,[8-10] and other ultrafast electrical devices, the need has arisen for a system of measurement capable of characterizing electrical signals with picosecond resolution. In the past, such electrical measurements have relied on sampling oscilloscopes whose temporal resolution is limited to approximately 25 ps. In 1980, Auston et al.[11] demonstrated a sampling technique in amorphous semiconductors that has recently achieved a temporal resolution of less than 3 ps,[18] limited by the carrier lifetime in the material. The use of the electro-optic effect for electrical signal characterization has for the most part been neglected because of the high voltages normally required to observe the Pockels effect.[12,13] Recently, we reported a new approach[14] to the characterization of electrical transients that exploits the speed of the electro-optic effect using sampling techniques[15] and a high-repetition-rate subpicosecond laser. That system used a lithium niobate traveling-wave Pockels cell as an ultrafast intensity modulator and achieved a temporal resolution of approximately 4 ps with a voltage sensitivity near 50 μV. We have since constructed several new modulators using lithium tantalate as the electro-optic medium. This crystal, superior to lithium niobate in several respects, has now enabled us to achieve subpicosecond temporal resolution with similar voltage sensitivity.

The Pockels effect lends itself to the characterization of electrical signals in many respects. First, and foremost, the mechanism respon-

sible for the Pockels effect, i.e., the polarizability to the electric field, has a temporal response in the femtosecond range and hence is not a limiting factor in picosecond operation. Second, the ability to use optical pulses directly to sample voltage levels allows the technique to benefit from the availability of ultrashort laser pulses. This optical arrangement also permits the effective use of velocity-matching techniques to enhance temporal resolution and sensitivity. This is described in more detail below. A third advantage of this approach is that the optical pulse probes the induced electric field without altering the circuit characteristics in any way, an important consideration when dealing with frequencies in the range of hundreds of gigahertz. Other advantages of electro-optic sampling are the large dynamic range of signals that can be measured (up to a few hundred volts), the wide spectral response of the Pockels cell, and the optical isolation of the detection electronics from the signal under investigation.

The system is depicted in Fig. 18 and utilizes a lithium tantalate traveling-wave Pockels cell between crossed polarizers as an ultrafast intensity modulator. A colliding-pulse mode-locked (CPM) laser[13] generating 120 fs pulses at 100 MHz is used to trigger the electrical signal source and synchronously sample the electric field induced by the unknown voltage as it propagates across the crystal. Two detectors are employed to measure the intensities of the transmitted and rejected beams at the analyzer. These signals are then processed by a differential amplifier,

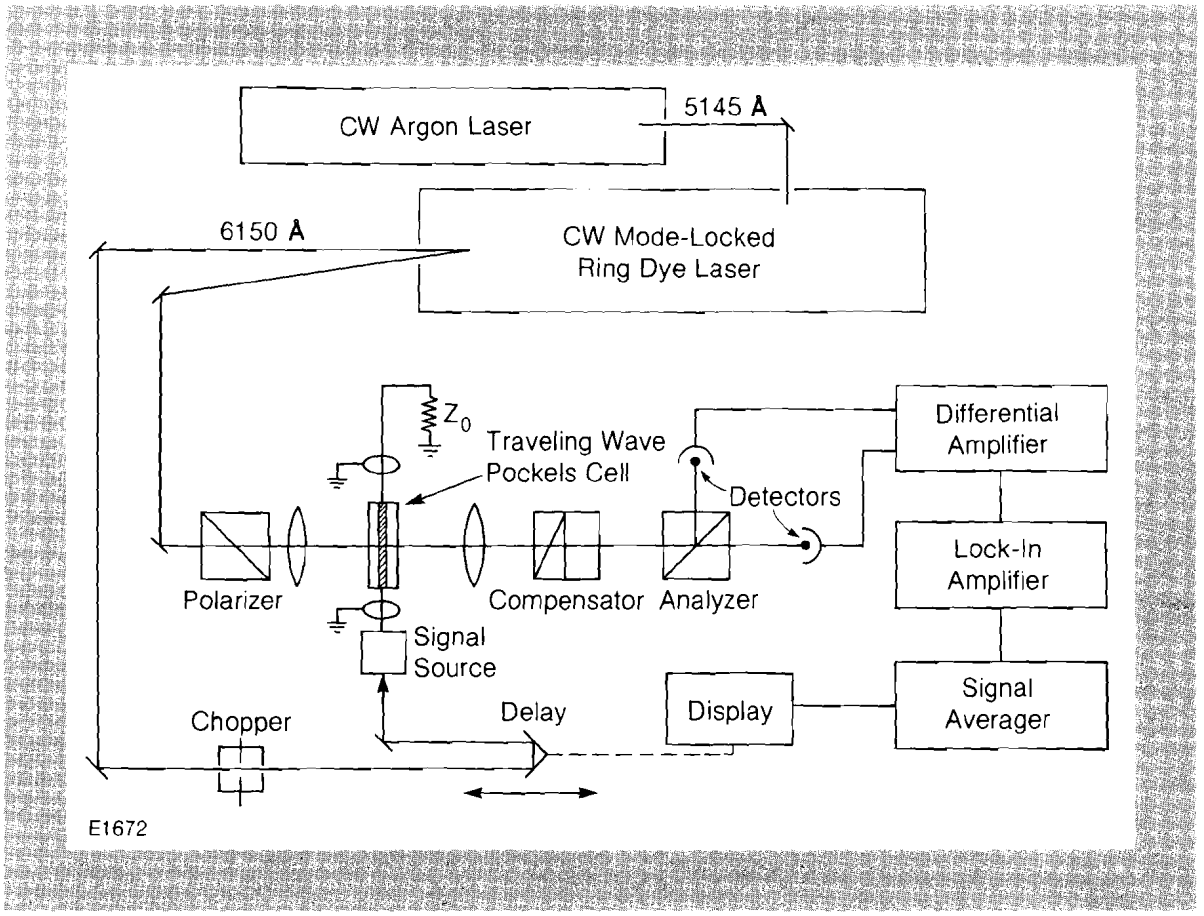

Fig. 18
Picosecond electro-optic sampling system layout.

lock-in amplifier, and signal averager. The differential system provides a means for making the detection system less susceptible to laser fluctuations while increasing the voltage sensitivity twofold. The modulator is optically biased, with a variable compensator at its quarter-wave point in order to achieve linear response as well as maximum voltage sensitivity. An optical delay line permits temporal scanning of the entire electrical profile by the optical probe pulse. The horizontal axis of the display is linearly driven in synchronism with the mechanical displacement of the delay line while the vertical axis is driven by the signal-averager output. This method results in a linear voltage versus equivalent time representation of the unknown electrical signal, requiring no further processing. Relatively slow detectors can be used since their necessary bandwidth is dictated only by the frequency of the light chopper used in conjunction with the lock-in detection system. This frequency is normally about 1 KHz.

The Pockels cell is a lithium tantalate crystal 0.7 mm wide by 0.25 mm thick by 15 mm long. Aluminum strip electrodes 0.3 mm wide are evaporated onto the two largest faces of the crystal, those being normal to the c-axis. This electrode geometry results in a balanced stripline with an impedance of ~45 ohms and a crystal half-wave voltage of nearly 2100 volts. The crystal is mounted between two subminiature coaxial-to-stripline microwave launchers with the optical beam focused through the 0.7 mm dimension. The beam size inside the crystal is optimally less than 20 μm, in order to obtain subpicosecond temporal resolution.

The properties of lithium tantalate as a traveling-wave modulator are superior to lithium niobate in several respects. The former has a much lower static birefringence, a decreased optical index of refraction, a higher threshold to optical damage, and a slightly enhanced electro-optic coefficient. The static birefringence of lithium tantalate has a value of 0.005, which is a factor of 18 less than its niobate counterpart. Thus, even though 100 fs optical pulses have a bandwidth of 50 Å, there is no need for a static birefringence compensator. The effects of temperature drifting are also minimized. The lower index of refraction ($n = 2.18$) makes it possible to achieve true velocity matching of the electrical and optical wavefronts. This configuration is crucial in obtaining subpicosecond performance.

The temporal resolution of the sampling head is determined by the convolution time of the optical probe pulse and the traveling electrical signal as they both propagate through the crystal. If these two signals travel orthogonally, the temporal resolution, τ_0, is the convolution of the time it takes for the probe pulse to traverse the crystal's electrodes with the transit time of the electrical signal across the probe beam waist. For a waist size of ~20 μm, the latter time is ~0.5 ps. The crystal traversal time is ~7 ps/mm. Thus, for our 0.3 mm electrode, the sampler would have a temporal resolution of 2.2 ps. However, this resolution can be reduced to the beam waist transit time by operating the crystal in the velocity-matching geometry. For this case, the probe beam enters the electro-optic crystal at an angle such that the optical velocity has a component in the same direction as the traveling electric field.

This geometry yields a fundamental resolution, or gating time, governed by the following equation:

$$\tau_0 = (w/c \cos \alpha)(n - \sqrt{\varepsilon} \sin \alpha) \quad (4)$$

where c is the speed of light in vacuum, n is the crystal index of refraction (~2.18), ε is the effective dielectric constant of the crystal, w is the electrode width, and α is the internal angle of incidence. In the present system, we obtain the best performance for $\alpha = 17$ degrees, indicating a fundamental temporal resolution in the order of 0.1 ps. Thus, we see that the beam waist size becomes the dominant factor and limits the expected resolution of this particular arrangement to approximately 0.5 ps.

The optimum temporal response is achieved with the optical probe beam entering the Pockels cell as close to the detector and upper electrode as is possible. This arrangement is necessary to minimize the electrical propagation distance, thereby limiting dispersion and preserving the ultrafast rise time of the detector.

Since this device uses the transverse electro-optic effect, the minimum voltage sensitivity is proportional to the ratio of electrode separation to the effective width seen by the probe beam, w/cos α. The Pockels cell was calibrated by applying a sine wave of known amplitude at the lock-in frequency. The measurement of the resultant intensity modulation yields the sensitivity at that frequency. To a first approximation, using published values of the S and T electro-optic coefficients, this value can be extrapolated to the microwave range. Sensitivity is fundamentally limited by the presence of laser noise at the lock-in frequency and hence is a strong function of the amount of signal averaging that is performed. The integration time necessary to achieve a given signal-to-noise ratio depends on scanning speed, scan length, and the resolution required. Typical times range from 5 seconds to several minutes for high-resolution operation. We have observed a voltage sensitivity of less than 50 μV, which is less than 10^{-7} of the half-wave voltage and corresponds to induced index changes of only 10^{-10}.

In order to verify the temporal performance of the sampling head, a suitably fast test signal is generated by a Cr-doped GaAs photoconductive detector. The detector is placed immediately adjacent to the Pockels cell under a common stripline,[13,14] with the photoconductive gap approximately 100-200 μm from the end of the crystal (see Fig. 19). When the detector is actuated by a 100 fs optical pulse, it generates an electrical pulse with an extremely fast rising edge containing frequencies up to many hundreds of gigahertz. Up to a certain cut-off frequency, determined by the physical parameters of the stripline geometry (in our cases, about 150 GHz), only the fundamental, quasi-TEM mode can propagate. Frequencies above this threshold can be transmitted not only as TEM modes, but also as higher-order TE and TM modes. Such modes, not forced to propagate parallel with the guiding electrodes, can arrive later at the sampling point, thus prolonging the total rise time of the generated signal. We are able to observe this phenomenon experimentally and have found that the relative delay between direct TEM

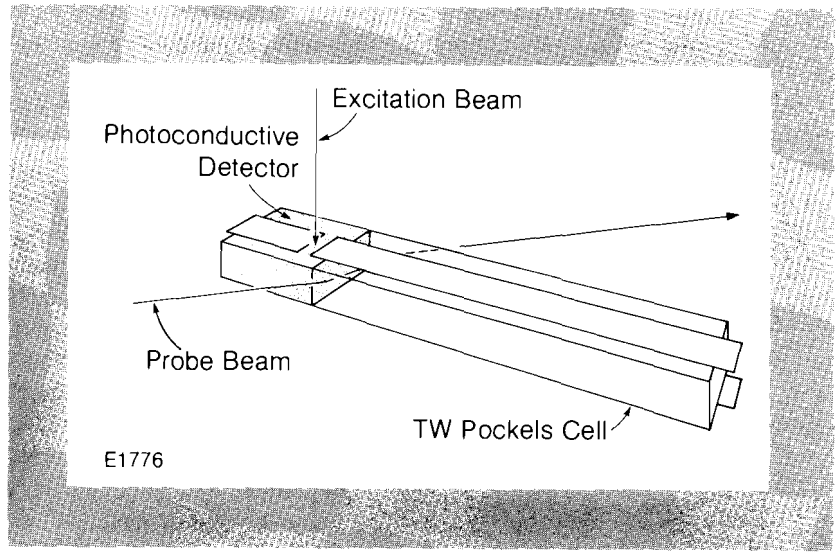

Fig. 19
Electro-optic crystal and detector test arrangement.

modes and indirect higher-order mode scales with sample substrate thickness, thus indicating a wave reflected from the ground plane. In order to avoid propagation of non-TEM, hybrid modes[17] in the range of frequencies up to 500 GHz, substrates and electrode dimensions of less than ~50 μm are required.

We present results that clearly demonstrate the relationship between the various parameters and that show how the resolution of the sampling gate is experimentally determined. Figure 20 shows the signal obtained from a switch built on a 500 μm substrate. An initial rise time of 2.4 ps is observed, followed by a secondary peak ~8 ps later. This delay corresponds very well with that of a wave reflected from the ground plane electrode, and confirms similar effects recently observed by Auston.[18] The ability of the sampling system to generate such a response curve,

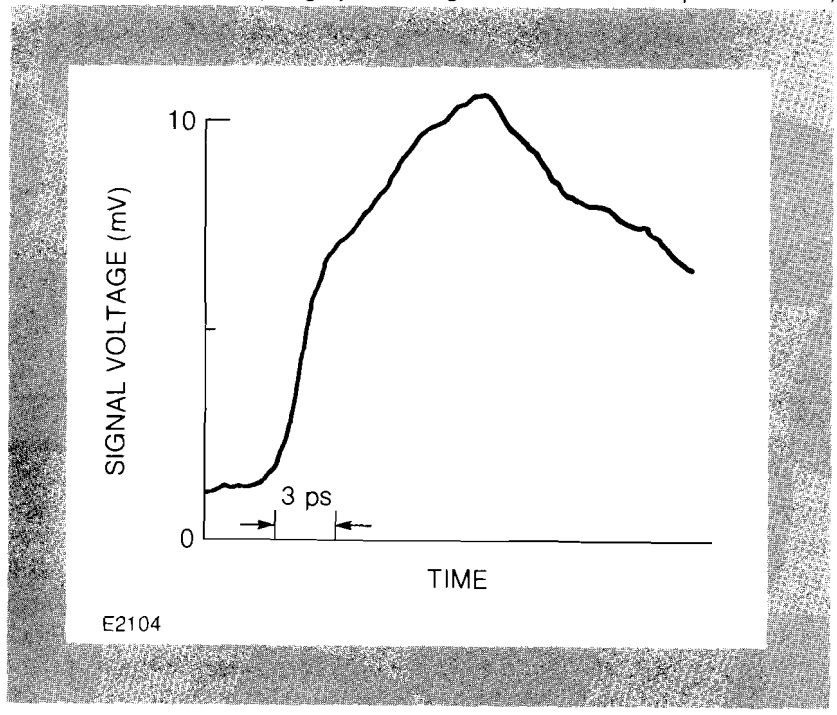

Fig. 20
Response of the Cr-doped GaAs photoconductive detector with 0.5 mm substrate thickness and 50 μm sampling beam diameter.

displaying an initial, steep, continuous rise without the presence of any slow leading edge, or foot, necessitates, from convolution theory, that the sampling gate function as a temporal duration at least as short as the rise time of the initial step. For this sampling head, the 10% to 90% time is ~2.4 ps. By reducing the substrate thickness to 250 μm, we expect the total rise time to be shortened, because the reflected wave incurs a shorter delay time. Figure 21(a) displays this result as a trace with an overall 10%-90% time of 2.3 ps. The direct and indirect waves are no longer resolved. By reducing the spot size of the sampling beam within the crystal (thus increasing the temporal resolution) we see—in Fig. 21(b)—that the two components can be resolved again while retaining the same overall rise time of ~2.3 ps. By reducing the spot size still further, to less than 20 μm, we reduce the electrical transit time across the beam waist to approximately 0.5 ps. Figures 21(c) and 22, respectively, show the rise time and actual trace obtained in this arrangement. The overall rise time is once again the same, as expected, but the direct wave now has a 10%-90% rise time of 850 fs, close to the predicted limit of 500 fs. The ability to resolve a rise time of 850 fs conclusively establishes the maximum possible width of the gating function. Thus, we see how the substrate thickness and beam size play separate roles in determining the overall rise time and resolution, respectively.

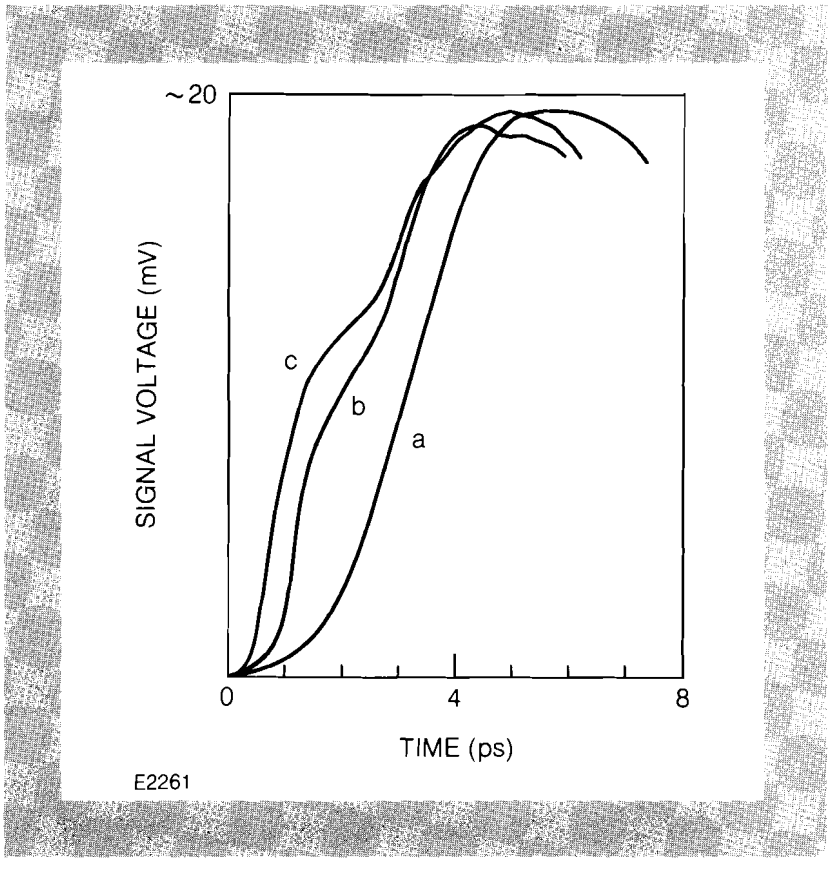

Fig. 21
Initial response of a Cr-doped GaAs photoconductive detector with 30 μm gap fabricated on a 0.25 mm substrate as a function of sampling beam diameter.
a) 50 μm
b) 25 μm
c) less than 20 μm

In short, we have developed an electro-optic sampling gate capable of characterizing electrical transients with subpicosecond resolution. Combining several conventional electronic instruments, we have been able to exploit the ultrafast response of the Pockels effect while retaining a voltage sensitivity of less than 10^{-7} of the crystal half-wave voltage.

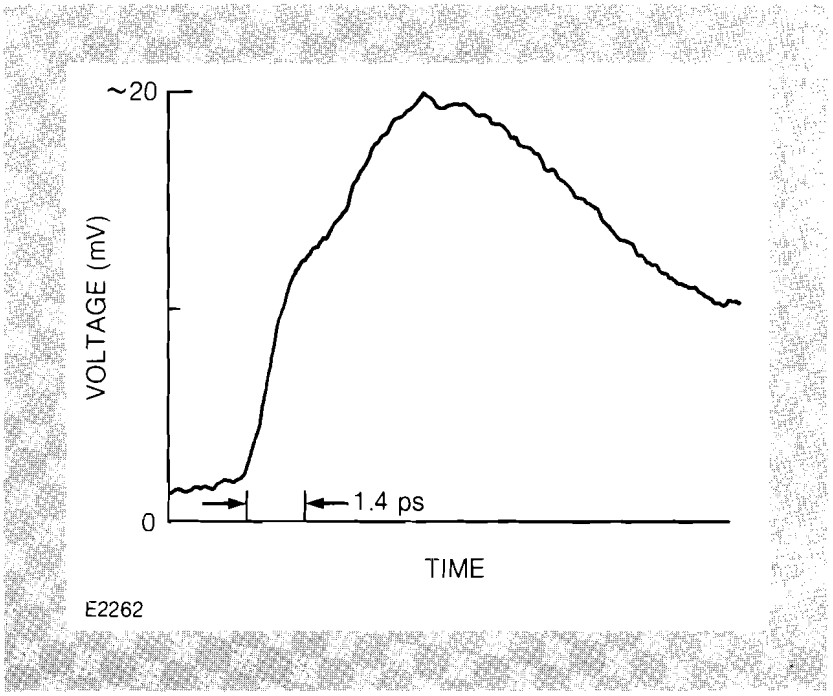

Fig. 22
Photograph of the actual display resulting from sampling the impulse response of a 30 μm gap Cr:GaAs photoconductive detector with a 250 μm substrate thickness. An initial rise time of 850 fs is clearly resolved, indicative of a comparable sampling time.

Also, it is important to emphasize that the temporal resolution of this system is not limited by the inherent response time of the active material but rather by the finite extent of the optical beam waist and the dispersive characteristics of the modulator striplines. Such a system now permits the possibility of analyzing ultrafast electrical processes such as those involved in photoconductive materials, photodetectors, and other picosecond electronic devices with the goal of understanding and improving their operation. Also, by employing high-repetition-rate, ultrafast electrical pulses that can now be well-characterized, it could be possible to reverse the roles of the optical and electrical signals in order to measure the performance of electrically-driven optical modulators[15] with picosecond resolution.

ACKNOWLEDGMENTS

We wish to thank Princeton Applied Research for supplying the signal averager and lock-in amplifier, and R. L. Fork for information leading to the stable operation of the CPM laser system.

We also acknowledge our debt to the technical expertise of Herb Graf for crystal fabrication and J. Drumheller and the target fabrication facility at LLE, for the crystal electrode coatings.

REFERENCES

1. R. A. Lawton and A. Scavennec, *Electron. Lett.* **11**, 74-75 (1975).
2. L. Green, *Rev. Sci. Instrum.* **47**, 1083-1085 (1976).
3. C. H. Lee, A. Antonetti, and G. Mourou, *Opt. Commun.* **21**, 158-161 (1977).
4. D. H. Auston, P. Lavallard, N. Sol, and D. Kaplan, *Appl. Phys. Lett.* **36**, 66-68 (1980).

5. P. R. Smith, D. H. Auston, A. M. Johnson, and W. M. Augustyniak, *Appl. Phys. Lett.* **38**, 47-50 (1981).

6. F. J. Leonburger and P. F. Moulton, *Appl. Phys. Lett.* **35**, 712-714 (1979).

7. A. P. Defonzo, *Appl. Phys. Lett.* **39**, 480-482 (1981).

8. D. H. Auston, *Appl. Phys. Lett.* **26**, 101-103 (1975).

9. C. H. Lee, *Appl. Phys. Lett.* **30**, 84-86 (1977).

10. G. Mourou and W. Knox, *Appl. Phys. Lett.* **35**, 492-495 (1979).

11. D. H. Auston, A. M. Johnson, P. R. Smith, and J. C. Bean, *Appl. Phys. Lett.* **37**, 371-373 (1980).

12. D. H. Auston and A. M. Glass, *Appl. Phys. Lett.* **20**, 398-399 (1972).

13. P. LeFur and D. H. Auston, *Appl. Phys. Lett.* **28**, 21-23 (1976).

14. J. A. Valdmanis, G. Mourou, and C. W. Gabel, *Appl. Phys. Lett.* **41**, 211-212 (1982).

15. R. C. Alferness, N. P. Economou, and L. L. Buhl, *Appl. Phys. Lett.* **37**, 597-599 (1980).

16. R. L. Fork, B. I. Greene, and C. V. Shank, *Appl. Phys. Lett.* **38**, 671-672 (1981).

17. J. J. Bahl and D. K. Trivedi, "A Designers Guide to Microstrip Line," *Microwaves*, May 1977.

18. D. H. Auston (private communication).

3.C High-Repetition-Rate Amplification of Subpicosecond Pulses

In the past, amplification of ultrashort optical pulses has been achieved through the use of high-energy nanosecond pump pulses generated by Nd:YAG,[1] nitrogen,[2] excimer, [3,4] and cavity-dumped argon-ion lasers.[5] In high-gain systems, the effective storage time due to fluorescence, molecular reorientation, and amplified spontaneous emission (ASE), does not exceed a few hundred picoseconds even for dye molecules with long fluorescence lifetimes. Therefore, in order to maximize the energy transfer between the pump and the dye laser pulses, it is important that the population inversion be established in a time significantly shorter than the effective storage time. In addition, the synchronization between the pump and dye laser pulses must be in the order of a fraction of the pump pulse width to take advantage of the peak gain.

A method of obtaining this synchronization is to drive the mode-lockers of two lasers with the same RF source. One laser is then used to synchronously pump a dye laser while the other is used to pump the amplifier. The dye laser produces pulses in the order of 100 fs at a repetition rate of 100 MHz.

The synchronous amplifier system was developed in order to provide a repetition rate high enough for signal averaging or lock-in techniques

with an output energy sufficient to observe nonlinear processes. The system layout is as shown in Fig. 23. Subpicosecond pulses from the synchronously-pumped dye laser are amplified in a single-pass two-stage configuration. The amplifier is pumped by an actively Q-switched and mode-locked CW Nd:YAG oscillator (Quantronix 114-R-O/QS ML) which is frequency-doubled in a temperature-tuned CD*A crystal. This oscillator can be triggered at rates up to 500 Hz while establishing a stable CW mode-locked oscillation (prelase) prior to Q-switching. This prelase ensures an output pulse stable both in amplitude and pulse-width.

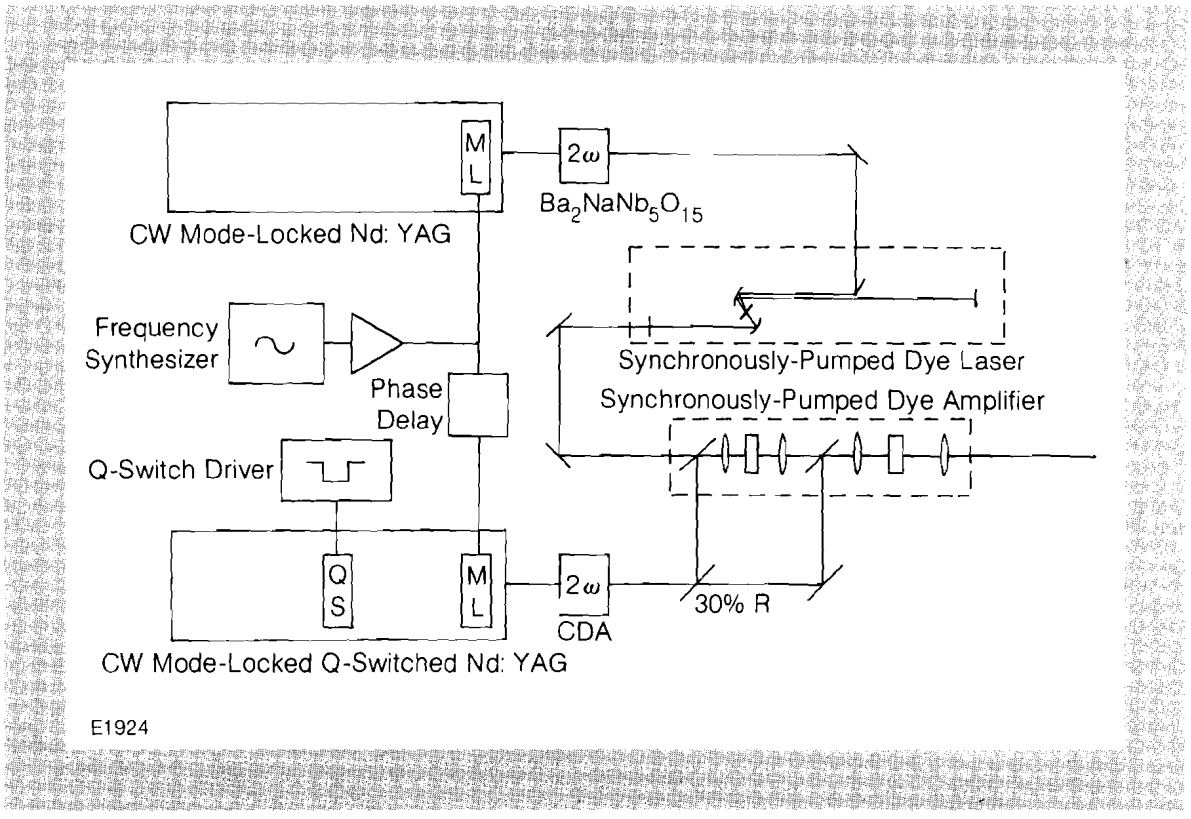

Fig. 23
Synchronized amplifier for femtosecond pulses using RF-coupled lasers.

To measure the timing accuracy (jitter) between the two pump lasers, the autocorrelation of each was taken. A Gaussian pulse shape was assumed to determine their respective pulse widths. The cross-correlation was then measured between the two lasers. The jitter was calculated, assuming a Gaussian distribution using,

$$\tau_{cc}^2 = \tau_1^2 + \tau_2^2 + \tau_j^2 \qquad (5)$$

where τ_{cc}, τ_1, τ_2, and τ_j are the full-width half-maximum widths of the cross-correlation, first laser, second laser, and the timing fluctuation respectively. In this manner the jitter is measured to be a maximum of 40 ps. There is a large uncertainty in this value due to the inherent difficulty in using the cross-correlation for jitter measurement; however, this value is viewed as an upper limit in light of previous work on mode-locked oscillator synchronization.[17] The autocorrelations of each pump laser and the cross-correlation between the two are as shown in Fig. 24 (this figure is included to illustrate the relative clarity of the data, not the relative widths, since the horizontal scales are not equal).

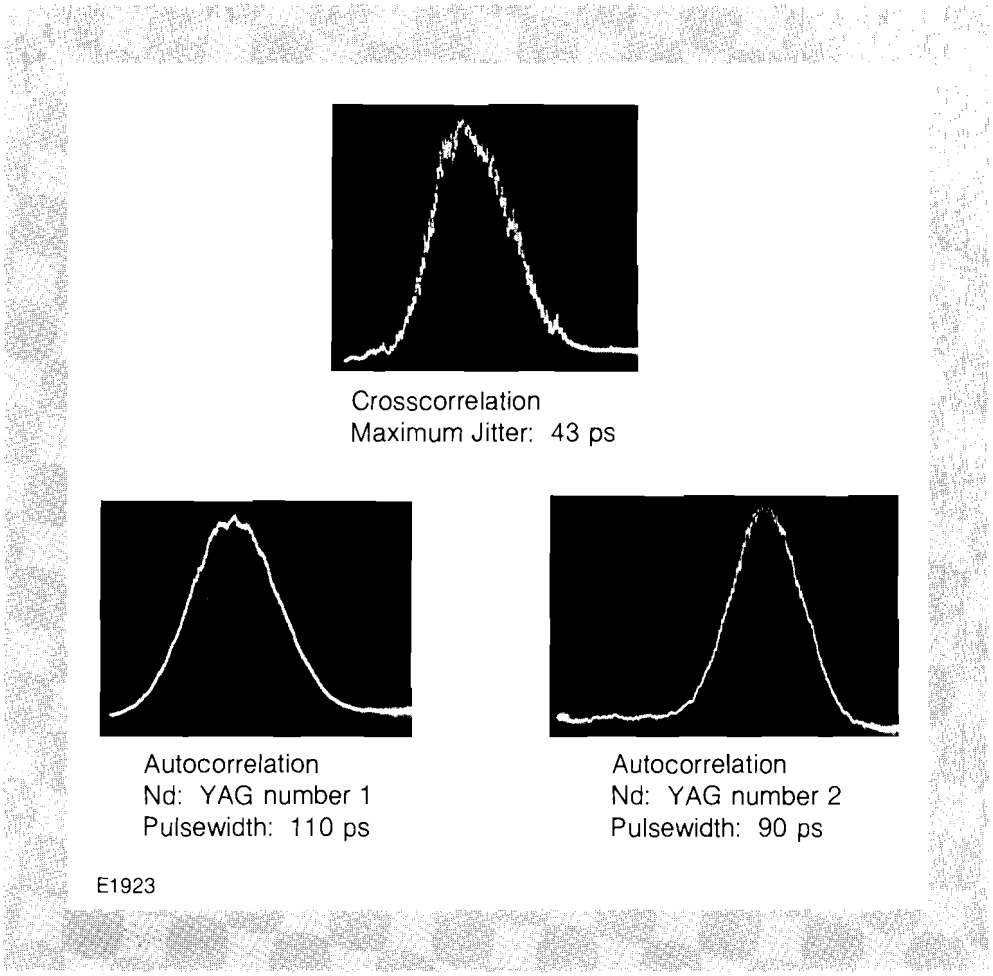

Fig. 24
Correlation measurement of the oscillator and amplifier pump laser to determine the relative timing.

The dye amplifiers were built using Kiton Red in water as the dye medium with 1 cm path lengths. The energy in the pump pulse is 25 μJ at 0.532 μm. Thirty percent of this energy is deposited in the first stage. Two amplifier stages are used in order to avoid the problem of heating during the train of pump pulses which would otherwise result in thermal blooming of the dye. This thermal problem is the limiting factor in the amplification. Output pulse energies of 350 nJ are obtained at 605 nm.

The thermal problem can be reduced by using a single pulse rather than the full train. Pulse selection has been accomplished either by a Pockels cell switchout external to the cavity or by cavity-dumping the pump laser. Single-pulse energies at 1.06 μm of 300 μJ have been obtained using a Pockels cell cavity dumper. The insertion loss of the dielectric polarizer and Pockels cell requires the prelase gain to be very close to threshold, significantly increasing the fluctuations in output energy.

The amplifier pump laser has a pulse amplitude peak stability of ± 1 % in a 25-pulse train. This stability is due to the better than 1 % regulation on the lamp current and the fact that a CW mode-locked prelase is established prior to Q-switching. By gating the Q-switch on a zero crossing of the carrier frequency (derived from the same synthesizer as the mode-locker RF), absolute timing between the Q-switch trigger and the

peak pulse is established allowing accurate triggering of a switchout. Amplitude fluctuation of the switched-out pulse is ± 1.5%.

To determine if the 40 ps jitter was small enough to do synchronous pumping, the gain depletion in the amplifier, shown in Fig. 25, was plotted by measuring the gain as a function of dye-laser-pulse delay. This delay was varied by changing the RF phase to the amplifier pump laser mode-locker, eliminating the need for an optical delay line. The measurement confirms that the synchronization is sufficient to amplify the pulse under peak gain conditions.

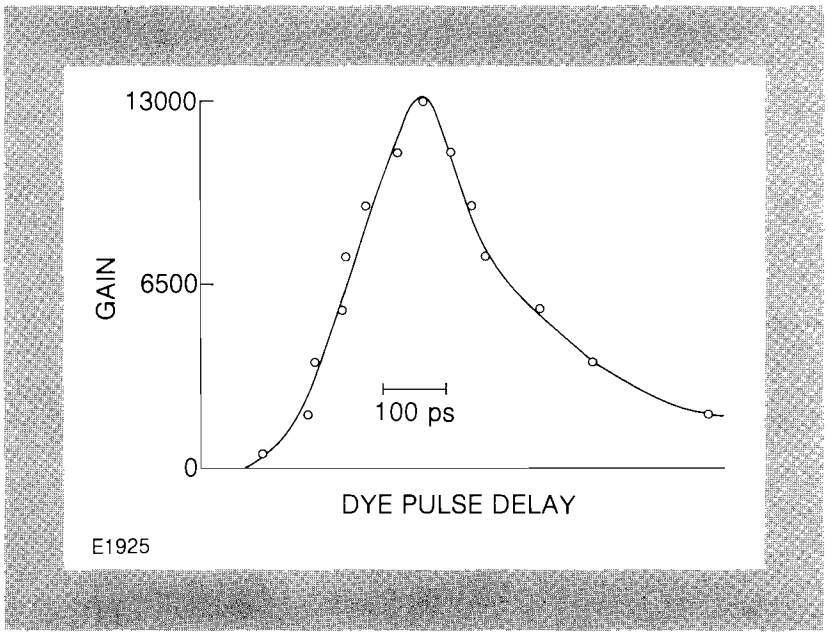

Fig. 25
Kiton Red amplifier (Fig. 23) gain versus time using the mode-locker RF phase to adjust the time delay.

The method of RF synchronization of two lasers can be generally applied to a wide range of systems, including the colliding-pulse mode-locked (CPM) laser,[8] provided that the mode-locker RF for the amplifier pump laser is derived from the CPM laser output and the cavity lengths of the two lasers are matched.

Synchronous pumping and amplification offer advantages as methods of femtosecond pulse generation and amplification. The benefits are particularly notable with regards to amplifying efficiency, decreased ASE, and the reduction of temporally-induced amplitude fluctuations. In addition, the synchronization between the amplifier pump pulse and the femtosecond pulse enables us to use the high-energy 1.06 μm pulse to drive detection electronics, such as jitter-free streak cameras,[9] or as an intense pump pulse for use in experiments.

REFERENCES

1. E. P. Ippen and C. V. Shank, "Subpicosecond Spectroscopy," *Picosecond Phenomena*, edited by C. V. Shank, E. P. Ippen, and S. L. Shapiro (Springer, Berlin, Heidelberg, New York, 1978), p. 103.
2. W. H. Hesselink and D. C. Wiersma, "Picosecond (Coherent) Transients in Molecular Mixed Crystals," *Picosecond Phenomena*, edited by C. V. Shank, E. P. Ippen, and S. L. Shapiro (Springer, Berlin, Heidelberg, New York, 1978), p. 192.

3. M. Maeda, T. Mizunami, A. Sato, O. Uchino, and Y. Miyazoe, *Appl. Phys. Lett.* **36**, 636 (1980).

4. P. B. Corkum and R. S. Taylor, *Appl. Phys.* **B28**, 248 (1982).

5. T. L. Gustafson and D. M. Roberts, *Opt. Commun.* **43**, 141 (1982).

6. G. A. Mourou and T. Sizer II, *Opt. Commun.* **41**, 47 (1982).

7. G. T. Harvey, C. W. Gabel, and G. Mourou, *Opt. Commun.* **36**, 213 (1981).

8. R. L. Fork, B. I. Greene, and C. V. Shank, *Appl. Phys. Lett.* **38**, 671 (1981).

9. W. Knox and G. Mourou, *Opt. Commun.* **37**, 203 (1981).

Section 4
NATIONAL LASER USERS FACILITY NEWS

This report covers the activities of the National Laser Users Facility (NLUF) during the quarter April to June 1982. During this period seven users conducted experiments on LLE facilities. The visiting scientists associated with these experiments represented UCLA, Yale University, the University of Maryland, the National Bureau of Standards, the Naval Research Laboratory, the University of Florida, the University of Illinois, and the University of Rochester. Also, during this period, the NLUF Steering Committee met to review and rank new proposals submitted by the users. Nine of the sixteen proposals were accepted, advancing the NLUF to a total of twenty-one user experiments.

Seven user experiments were conducted during this quarter, compiling a total of 317 shots on the Glass Development Laser (GDL) and the OMEGA laser systems. Table 1 gives a summary of the number of shots for each user experiment.

The GDL laser system accommodated four user experiments during the quarter. Typically, the laser system delivered 35 Joules of 0.35 μm laser light in a nanosecond pulse. The laser was focused onto flat targets for either plasma physics or x-ray diffraction experiments. Research scientists from the following four institutions participated in the experiments:

1. Francis Chen, Chan Joshi, and Humberto Figueroa (UCLA), and Nizarali Ebrahim and Hiroshi Azechi (Yale University).

2. Hans R. Griem and John Adcock (University of Maryland), Joseph Reader (National Bureau of Standards), and Uri Feldman (Naval Research Laboratory).
3. Anthony Burek (National Bureau of Standards) and Barukh Yaakobi (University of Rochester).
4. James Forsyth and Robert Frankel (University of Rochester).

User System Shot Distribution
April 1 to June 30, 1982

USER (Principal Investigator)	FACILITY	NUMBER OF SHOTS
UCLA & Yale University (F. Chen)	GDL	78
University of Maryland (H. Griem)	GDL	12
National Bureau of Standards (A. Burek)	GDL	19
University of Rochester (J. Forsyth)	GDL	65
Naval Research Laboratory (U. Feldman)	OMEGA	26
University of Florida (C. F. Hooper, Jr.)	OMEGA	55
University of Illinois (G. Miley)	OMEGA	60
University of Rochester (B. Yaakobi)	OMEGA	2
	TOTAL	317

U57

Table 1
User system shot distribution from April 1 to June 30, 1982.

The UCLA/Yale experiment accumulated 78 system shots during this quarter (in the previous quarter they received 17 experimental shots plus 25 diagnostic check-out shots). The objective of the experiment is to study the effects of specific instabilities in producing energetic electrons or scattering of the laser light. [The specific instabilities are Stimulated Raman Scattering (SRS) and two-plasmon decay.] These instabilities occur at densities less than or equal to quarter-critical (at an electron density of 2×10^{21} for 0.35 μm laser light). A long scale-length plasma is used to simulate the conditions expected in reactor-sized targets. The long scale-length is formed by focusing two pulses, separated by 1 ns, onto a foil target. The first pulse has an energy of approximately 7 J at 1.054 μm and forms the long scale-length plasma. The second pulse has an energy of 35 J at 0.35 μm and is used to study the instabilities. The spot size of the 1.054 μm beam was 1 mm, producing an irradiance of 5×10^{11} W/cm^2. The 0.35 μm beam was tightly focused to 70 μm diameter, yielding an irradiance of 10^{15} W/cm^2. This special optical arrangement was provided by members of the LLE scientific staff.

The diagnostics for the experiment consisted of a user-supplied, visible spectrograph to examine the Raman spectrum and two electron spectrometers for the angular distribution of hot electrons. Other diag-

nostics supplied by LLE included an additional visible spectrograph, and six calibrated photodiodes to monitor the angular distribution of $\omega_0/2$ light.

The University of Maryland experiment was completed with twelve shots in this quarter. (They had 32 shots in the previous quarter.) The goal of the experiment is to examine the broadening and wavelength shifts of the soft x-ray line emission from a laser-produced plasma. An understanding of these spectral features can be used to diagnose the plasma temperature and density.

The experimental configuration used a 0.35 μm laser pulse focused onto foils of different elements. A soft x-ray spectrometer, previously flown in solar physics experiments, was used to record the spectrum. The spectrometer was supplied by the Goddard Space Flight Center. The instrument is a 3 m, grazing-incidence spectrograph capable of covering a wavelength range of 8 to 780 Å. A single shot easily produced well-exposed spectra. Spectra were taken of carbon, oxygen, fluorine, iron, niobium, molybdenum, and silver.

The experiment by the National Bureau of Standards used 19 shots to test the application of a Laue-type, x-ray diffracting crystal for target-implosion diagnostics. In a Laue crystal, x-ray radiation passes through the crystal instead of reflecting, as in a Bragg Geometry. The entire spectrum goes through a "focus", allowing a reduction in the background radiation by appropriate placement of an aperture. Figure 26 shows the geometry of a Laue-type spectrograph.

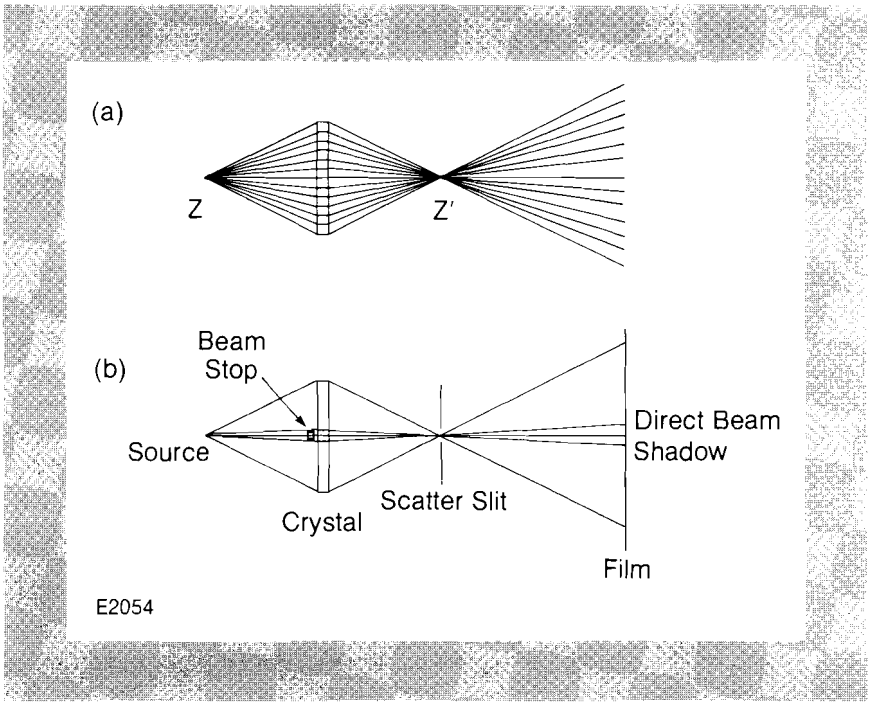

Fig. 26
Configuration of a Laue-type x-ray diffraction spectrometer.
a) a ray trace of x-rays diffracted by the crystal
b) compounds in the diagnostic

A Laue-type spectrograph was constructed by the National Bureau of Standards and used to examine a titanium spectrum produced from a laser plasma. Figure 27 shows typical titanium spectra recorded (on different shots) using Laue- and Bragg-type spectrographs. The spectra

show both helium-like and hydrogenic spectra, including resonance lines and satellites. The line ratios are different in the two examples; the Laue experiment used a larger laser focal spot which produced a lower plasma electron temperature. Also, the spectral dispersion is different for the two examples; this accounts for the closer spacings of lines in the Laue geometry. In other respects the Laue spectrogram exhibits features comparable to the features in the Bragg spectrogram.

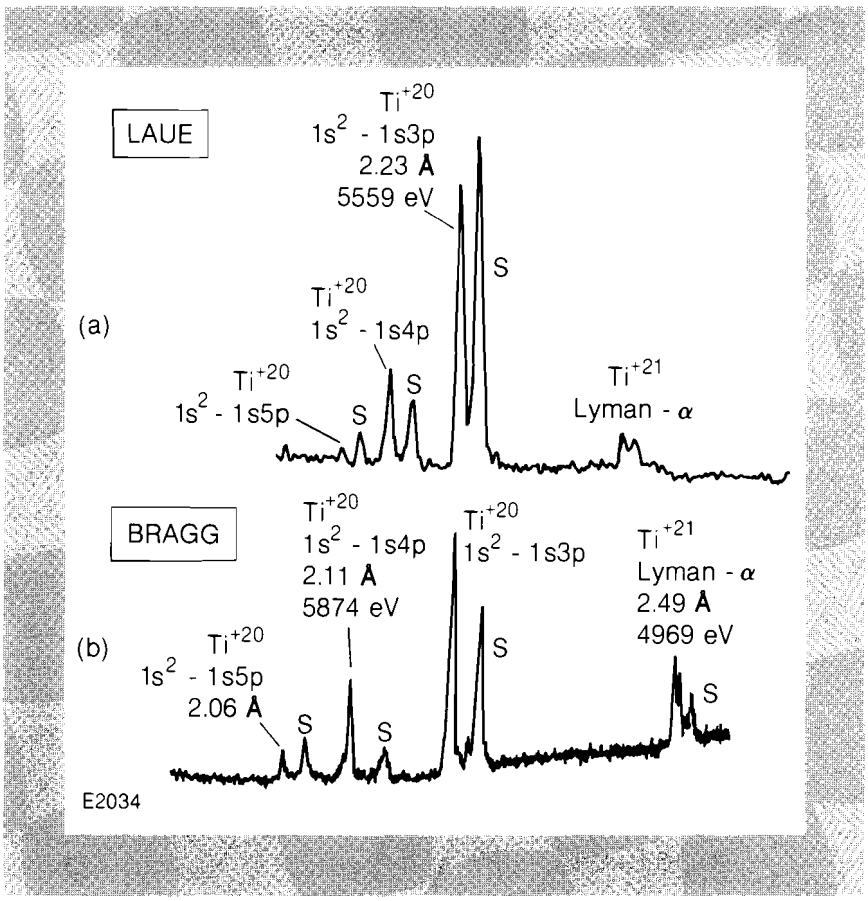

Fig. 27
A comparison of Laue and Bragg x-ray spectrographs.
a) spectrum of titanium using a Laue spectrograph
b) spectrum of titanium using a Bragg spectrograph

A Laue spectrograph may be used as a diagnostic for compression measurements in laser-fusion experiments. This application uses x-rays to backlight a fusion target and measure the x-ray transmission. An example of this technique is shown in Fig. 28. This figure shows the x-ray transmission of a 420 μm diameter CH_2 sphere placed at the Laue focus. The x-rays used for this example are at 4.750 keV from the $1s^2$-1s2p Ti^{+20} line. The measured x-ray transmission compares well with the calculation.

The University of Rochester experiment conducted by Jim Forsyth and Robert Frankel uses x-rays from a laser-plasma source for kinetic x-ray diffraction experiments. Preliminary results from this experiment were reported in LLE Review, Volume 8. During this quarter, target shots were used to test upgrades of the diagnostic equipment.

The remaining four user experiments were conducted on the OMEGA facility. The system was operated at a nominal pulse width of 100 ps and typically delivered 600 Joules on target. In most of the experiments, all

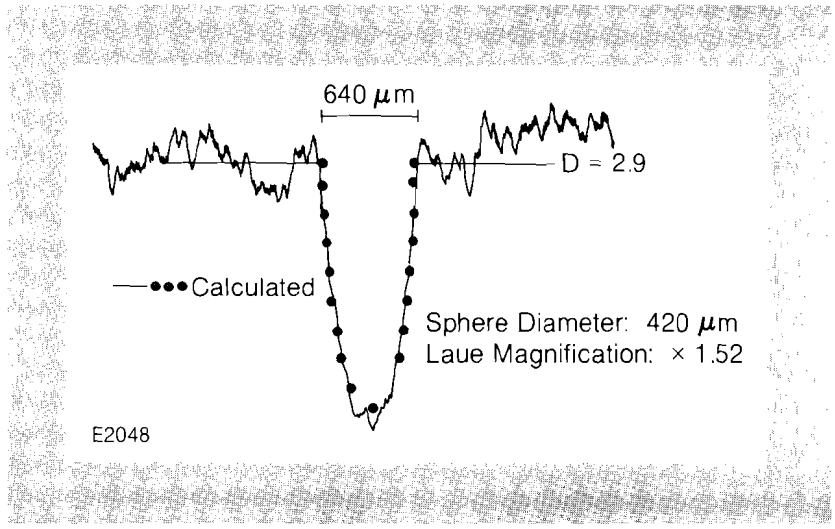

Fig. 28
Backlighting of a CH_2 sphere in a Laue geometry. A monochromatic image is shown using 4.750 keV x-rays produced from a titanium target.

24 beams of the OMEGA laser were focused onto thin-wall glass microballoons. Research scientists associated with the following institutions participated in the experiments:

1. Uri Feldman and George Doschek (Naval Research Laboratory) and W. E. Behring (Goddard Space Flight Center).
2. C. F. Hooper, Jr. (University of Florida); Natale Ceglio, Robert Kauffman, Gary Stone, and Gary Howe (Lawrence Livermore National Laboratory); Andrew Hawryluk (MIT); and Stan Skupsky and Barukh Yaakobi (University of Rochester).
3. George Miley, Chan Choi, Aaron Bennish, and David Harris (University of Illinois).
4. Barukh Yaakobi (University of Rochester) and H. W. Schnopper and P. O. Taylor (Smithsonian Institution).

The Naval Research Laboratory experiment received 26 shots in this quarter. Dr. Feldman and his colleagues studied the soft x-ray emission from spherical targets irradiated by the OMEGA laser system. The goal of the experiment is to identify the line emission from high-Z elements in order to develop an application of spectroscopic diagnostics of inertial fusion conditions. This application will be useful in examining the density and temperature in the lower temperature region of the plasma. X-rays emitted from the lower temperature plasma regions will tend to originate in lower ionization stages and the emission will tend to be concentrated in the soft x-ray region of the spectrum.

The configuration for the experiment was to focus all 24 beams from the OMEGA system onto spherical targets composed of different elements. The spectrograph is the same one used in the University of Maryland experiments. The targets were glass microballoons with coatings of titanium, copper, parylene, or gold. One type of target was filled with krypton gas. (Details of the target coating and filling procedures can be found in LLE Review, Volumes 7 and 8.) A soft x-ray spectrum was recorded for each of the above types of targets.

The University of Florida experiment received 55 shots to examine the physics of x-ray line profiles in laser fusion experiments. A measurement of these x-ray line profiles is useful in determining plasma conditions, such as density and fuel ρR.

The experiment consisted of irradiating spherical microballoons filled with either argon gas or a mixture of argon and neon. Various pressures of the gas mixtures were used to examine the effects of argon cooling in the implosions. Diagnostics for the experiment examined the x-ray emission from both the gas and the glass components.

Several of the diagnostics were supplied by Lawrence Livermore National Laboratory, including a zone-plate-coded image camera,[1] and transmission x-ray gratings. The total x-ray diagnostic complement included (1) a zone-plate-coded image camera to evaluate the sphericity of the implosion (the diagnostic covers a range of approximately 3 to 30 keV, in five distinct energy bands, with a spatial resolution of 4-8 microns); (2) time- and spatially-resolved x-ray spectroscopy measurements using transmission x-ray gratings (covering a range of 500 eV to 5 keV) employed with an LLE-supplied x-ray streak camera for temporal resolution, and with an LLE-supplied grazing-incidence reflection microscope for spatial resolution; and (3) two flat crystal (LLE) x-ray spectrometers to examine the line emission of silicon, neon, and argon.

The University of Illinois experiment was completed in this quarter with 60 shots on the OMEGA facility. This experiment was designed to examine the energy loss of fusion-reaction products as they passed through the outer parts of the expanding plasma. These fusion products act as "test particles" since they are emitted in a short time, compared with the time taken for the total target implosion.

The experimental diagnostic was a particle time-of-flight spectrometer capable of measuring the 3.5 MeV alpha particles emitted in DT reactions and the 3.0 MeV protons emitted from DD reactions. Spherical microballoons were filled with a mixture of deuterium and tritium in the ratio of 95% deuterium to 5% tritium at a pressure of 20 atmospheres. This mixture was chosen to enhance the 3 MeV proton signal since the DD reaction rate is approximately 1/100 of the DT reaction. Data was recovered for a variety of target diameters and wall thicknesses to examine the particle energy losses as a function of target mass.

The University of Rochester experiment consisted of two dedicated and fourteen shared shots to test a focusing x-ray crystal spectrometer. This curved-crystal, x-ray spectrometer is a "Von-Hamos" type, designed to focus the x-ray emission, and hence provide increased sensitivity over flat crystals. Thus, reduced amounts of a tracer gas can be added to the target while still recording the tracer x-ray emission.

The experiment attempted to record the emission from a variety of elements in typical implosion experiments. Elements of krypton, germanium, silicon, and copper were used. Krypton gas was filled inside a glass microballoon, and the other elements were coated onto the glass. A preliminary examination of the x-ray spectra shows lines from all of the

elements. Especially interesting is the ability to record the Lyman-α hydrogenic line (1s-2p) and heliogenic lines of copper and germanium. The heliogenic $1s^2$-1s2p line of krypton was also recorded.

These experiments were supported by contracts with the U.S. Department of Energy, except for J. M. Forsyth's work, which is supported by the National Science Foundation and the National Institutes of Health.

The targets used by the Naval Research Laboratory (Uri Feldman), University of Florida (C. F. Hooper, Jr.), University of Illinois (George Miley), and the University of Rochester (Barukh Yaakobi) were supplied by KMS Fusion, Inc. and by the University of Rochester's Laser Fusion Feasibility Project. The targets used by the University of Maryland (Hans Griem) and the National Bureau of Standards (Anthony Burek) were supplied by the University of Rochester's Laser Fusion Feasibility Project.

Future issues of the LLE Review will highlight additional results from user experiments performed in this quarter.

During this quarter, on June 4, 1982, the NLUF Steering Committee had their third meeting, to review and approve proposals, and to recommend funding of approved proposals to the Department of Energy. The Committee membership remained the same as that at the previous meeting, consisting of scientists from a broad range of areas, including laser fusion, atomic physics, plasma physics, astrophysics, biophysics, and materials research. The Committee membership consists of Dr. David T. Attwood, Jr. (Lawrence Livermore National Laboratory), Dr. Michael Bass (University of Southern California), Dr. Manfred A. Biondi (University of Pittsburgh), Dr. Thomas C. Bristow (non-voting Executive Secretary, University of Rochester), Dr. Donald L. D. Caspar (Brandeis University), Dr. Lamar W. Coleman (absent, Lawrence Livermore National Laboratory), Dr. Gordon P. Garmire (Pennsylvania State University), Dr. Hans R. Griem (University of Maryland), and Dr. Brian J. Thompson (Chairman, University of Rochester).

The Committee approved 9 of 16 proposals for user experiments. The approved experiments are in areas of laser fusion, plasma physics, and x-ray biophysics. These new proposals are from the following investigators:

1. NLUF Proposal 36: R. Elton (Naval Research Laboratory), "Gain Measurements for a Soft X-Ray Laser High-Density Plasma Probe."
2. NLUF Proposal 40: Leo G. Herbette (University of Connecticut), "Time-Resolved X-Ray Diffraction of Acetylcholine Receptor Membranes."
3. NLUF Proposal 41: J. K. Blasie (University of Pennsylvania), "Time-Resolved Structural Studies of the Ca^{2+}-ATPase of Sarcoplasmic Reticulum Membranes Utilizing a Laser Plasma X-Ray Source."

4. NLUF Proposal 42: U. Feldman (Naval Research Laboratory), "Measurements of Spatially-Resolved High-Resolution Spectra of Laser-Produced Plasmas Using the OMEGA Laser Facility at the University of Rochester."
5. NLUF Proposal 43: T. Blue (University of Illinois), "Measurement of D-^{3}He Proton Yield With CR-39 as a Diagnostic for Inertial Confinement Fusion Experiments."
6. NLUF Proposal 44: H. Griem (University of Maryland), "Shifts and Widths of Hydrogenic Ion Lines: Experimental Proposal for Continuation of Measurements at the University of Rochester Laser Users Facility."
7. NLUF Proposal 46: B. Henke (University of Hawaii), "Development and Evaluation of a Streak-Camera-Coupled Elliptical-Analyzer Spectrograph System for the Diagnostics of Laser-Driven X-Ray Sources (100-10,000 eV Region)."
8. NLUF Proposal 48: F. Chen (UCLA), "Studies of the Two-Plasmon Decay and Stimulated Raman-Scattering Instabilities in Hot, Long Scale-Length Plasmas."
9. NLUF Proposal 49: C. F. Hooper, Jr. (University of Florida), "Implosion Dynamics of the Fuel, Pusher, and Fuel-Pusher Interface."

Further information on the NLUF is available by writing to:

Thomas C. Bristow, Manager
National Laser Users Facility
Laboratory for Laser Energetics
University of Rochester
250 East River Road
Rochester, New York 14623

REFERENCES

1. N. M. Ceglio, D. T. Attwood, and J. T. Larsen, *Phys. Rev. A* **25**, 2351 (1982); N. M. Ceglio, A. M. Hawryluk, and R. H. Price, *Proc. SPIE* **316**, 134 (1982).

PUBLICATIONS AND CONFERENCE PRESENTATIONS

Publications

G. F. Albrecht, "Temporal Shape Analysis of Nd:YLiF Active Mode-Locked/Q-Switched Oscillator," *Opt. Commun.* **41**, 287-291 (1982).

D. Glocker and R. Wiseman, "A New Method for the Batch Production of Micro-Fresnel Zone Plates," *J. Vac. Sci. Technol.* **20**, 1098-1100 (1982).

D. A. Glocker, J. P. Drumheller, and J. R. Miller, "Ion Beam Sputter Deposition onto Levitated and Stalk-Mounted Laser Fusion Targets," *J. Vac. Sci. Technol.* **20**, 1331-1335 (1982).

T. F. Powers, "Improved Nonconcentricity Characterization of Transparent Laser Fusion Targets by Interferometry," *J. Vac. Sci. Technol.* **20**, 1355-1358 (1982).

B. A. Brinker and J. R. Miller, "Capillary Gas Filling of Inertial Fusion Targets," *J. Vac. Sci. Technol.* **20**, 1079-1081 (1982).

G. Mourou, W. Knox, and S. Williamson, "Picosecond High-Power Switching and Applications," *Laser Focus Magazine*, 97-106 (April 1982).

K. Tanaka, L. M. Goldman, W. Seka, M. C. Richardson, J. M. Soures, and E. A. Williams, "Stimulated Raman Scattering from UV-Laser-Produced Plasmas," *Phys. Rev. Lett.* **48**, 1179-1182 (1982).

B. Yaakobi, J. Delettrez, L. M. Goldman, R. L. McCrory, W. Seka, and J. M. Soures, "Preheat Measurements in UV-Laser Target Interaction," *Opt. Commun.* **41**, 355-359 (1982).

S. Williamson, G. F. Albrecht, and G. Mourou, "Laser-Triggered Cr:GaAs HV Sparkgap with High Trigger Sensitivity," *Rev. Sci. Instrum.* **53**, 867-870 (1982).

Forthcoming Publications

G. Mourou and S. Williamson, "Picosecond Electron Diffraction," accepted for publication by *Applied Physics Letters*.

G. Mourou, W. Knox, and S. Williamson, "Advances in Picosecond Optoelectronics," accepted for publication by *S.P.I.E., Picosecond Lasers and Application*.

H. Kim, T. F. Powers, and J. Mason, "Real-Time Parylene Coating Thickness Measurement Using Optical Reflectrometry," accepted for publication by *Journal of Vacuum Science Technology*.

C. P. Verdon and R. L. McCrory, "Nonlinear Effects of Multifrequency Hydrodynamic Instabilities on Ablatively Accelerated Thin Shells," accepted for publication by *Physics of Fluids*.

S. Kacenjar, S. Skupsky, A. Entenberg, L. M. Goldman, and M. C. Richardson, "Direct Measurement of the Fuel Density-Radius Product in Laser-Fusion Experiments," accepted for publication by *Physical Review Letters*.

B. Yaakobi, D. M. Villeneuve, M. C. Richardson, J. M. Soures, R. Hutchison, and S. Letzring, "X-Ray Spectroscopy Measurements of Laser-Compressed, Argon-Filled Shells," accepted for publication by *Optics Communications*.

G. Weyl, D. Rosen, J. Wilson, and W. Seka, "Laser-Induced Breakdown of Argon at 0.35 μm," accepted for publication by *Physical Review A: General Physics*.

R. W. Short, R. Bingham, and E. A. Williams, "Filamentation of Laser Light in Flowing Plasmas," accepted for publication by *Physics of Fluids*.

J. Reynolds, "Information Management Data Base for Fusion Targets," accepted for publication by *Journal of Vacuum Science and Technology*.

S. Sarraf, E. A. Williams, and L. M. Goldman, "Ion-Ion Two-Stream Instability in Multispecies Laser-Produced Plasma," accepted for publication by *Physical Review A: General Physics*.

Conference Presentations

J. A. Abate, S. D. Jacobs, W. S. Piskorowski, and T. P. Pottenger, "Spatially Resolved Characterization of Thin Films," presented at the Annual Meeting of the Conference on Lasers and Electro-Optics, Phoenix, Arizona, April 1982.

G. F. Albrecht, "Temporal Shape Analysis of Mode-Locked/Q-Switched Nd^{3+} Laser Pulses," presented at the Annual Meeting of the Conference on Lasers and Electro-Optics, Phoenix, Arizona, April 1982.

T. Sizer II, J. D. Kafka, and G. Mourou, "Generation and Amplification of Seventy Femptoseconds Using a Frequency-Doubled Nd:YAG Pumping Source," presented at the Annual Meeting of the Conference on Lasers and Electro-Optics, Phoenix, Arizona, April 1982.

J. M. Forsyth, "Applications of Laser-Produced Plasma X-Ray Radiation in Structural Kinetic Studies," presented at the Annual Meeting of the Conference on Lasers and Electro-Optics, Phoenix, Arizona, April 1982.

J. Hoose, R. Hopkins, L. Lund, S. Kumpan, and W. Friedman, "Phase and Intensity Measurements of the Omega Laser System," presented at the Annual Meeting of the Conference on Lasers and Electro-Optics, Phoenix, Arizona, April 1982.

M. C. Richardson, B. Yaakobi, J. Delettrez, D. M. Villeneuve, S. Letzring, A. Entenberg, R. S. Marjoribanks, S. Kacenjar, and J. M. Soures, "Final Core Conditions of Symmetrically Imploded Large-Aspect-Ratio Targets," presented at the Annual Meeting of the Conference on Lasers and Electro-Optics, Phoenix, Arizona, April 1982.

J. M. Soures, "Short-Wavelength Direct-Drive Laser Fusion: A Status Report," invited paper presented at the Annual Meeting of the Conference on Lasers and Electro-Optics, Phoenix, Arizona, April 1982.

J. M. Soures, "Laser-Matter Interaction Studies at the University of Rochester Laboratory for Laser Energetics," presented at the Japan-U.S. Seminar on Theory and Application of Multiply-Ionized Plasmas Produced by Laser and Particle Beams, Nara, Japan, May 1982.

L. D. Lund, "Construction of the Omega Laser System," presented at the Optical Society Spring Meeting on Applied Optics, Rochester, New York, May 1982.

A. Simon, E. Williams, T. Dewandre, and R. L. McCrory, "Improved Threshold Criteria for the Inhomogeneous $2\omega_p$ Instability," presented at the Twelfth Annual Conference on Anomalous Absorption of Electromagnetic Waves, Sante Fe, New Mexico, May 1982.

D. M. Villeneuve, W. Friedman, J. Hoose, M. C. Richardson, S. Letzring, R. Hutchison, K. Lee, S. Skupsky, R. L. McCrory, and J. M. Soures, "Irradiation Uniformity of Spherical Targets on OMEGA," presented at the Twelfth Annual Conference on Anomalous Absorption of Electromagnetic Waves, Sante Fe, New Mexico, May 1982.

R. S. Craxton and R. L. McCrory, "Two-Dimensional Hydrodynamic Effects in Single Beam Laser-Plasma Interaction Experiments," presented at the Twelfth Annual Conference on Anomalous Absorption of Electromagnetic Waves, Sante Fe, New Mexico, May 1982.

J. Delettrez, B. Yaakobi, M. C. Richardson, T. Boehly, R. S. Marjoribanks, S. Letzring, R. Hutchison, R. L. McCrory, J. M. Soures, and G. D. Enright, "Energy Transport and Partitioning in Nanosecond One-Micron Spherical Target Irradiation Experiments," presented at

the Twelfth Annual Conference on Anomalous Absorption of Electromagnetic Waves, Sante Fe, New Mexico, May 1982.

R. Epstein and R. S. Craxton, "First-Order Refractive Effects of Density Fluctuations on Light Rays in a Plasma," presented at the Twelfth Annual Conference on Anomalous Absorption of Electromagnetic Waves, Sante Fe, New Mexico, May 1982.

R. L. Keck, L. M. Goldman, M. C. Richardson, W. Seka, K. Tanaka, D. Villeneuve, and E. A. Williams, "Coronal Electron Temperature Measurements in UV-Laser Plasmas," presented at the Twelfth Annual Conference on Anomalous Absorption of Electromagnetic Waves, Sante Fe, New Mexico, May 1982.

P. Koch and E. A. Williams, "The Raman Instability Can Be Absolute Below Quarter-Critical," presented at the Twelfth Annual Conference on Anomalous Absorption of Electromagnetic Waves, Sante Fe, New Mexico, May 1982.

R. L. McCrory, C. P. Verdon, K. Lee, J. Delettrez, M. C. Richardson, D. M. Villeneuve, and J. M. Soures, "Theoretical Interpretation of Multi-Dimensional Effects of OMEGA Uniformity Experiments," presented at the Twelfth Annual Conference on Anomalous Absorption of Electromagnetic Waves, Sante Fe, New Mexico, May 1982.

M. C. Richardson, S. Letzring, D. M. Villeneuve, B. Yaakobi, A. Entenberg, S. Kacenjar, R. Marjoribanks, R. Hutchison, J. Delettrez, R. L. McCrory, and J. M. Soures, "Uniform Compression of Large-Aspect-Ratio Targets Driven by Nanosecond, 24-Beam Laser Pulses from OMEGA," presented at the Twelfth Annual Conference on Anomalous Absorption of Electromagnetic Waves, Sante Fe, New Mexico, May 1982.

J. E. Rizzo, S. Letzring, and M. C. Richardson, "Harmonic Emission from Uniformly Illuminated Spherical Targets," presented at the Twelfth Annual Conference on Anomalous Absorption of Electromagnetic Waves, Sante Fe, New Mexico, May 1982.

W. Seka, L. M. Goldman, M. C. Richardson, J. M. Soures, D. M. Villeneuve, B. Yaakobi, R. S. Craxton, J. Delettrez, R. L. McCrory, R. Short, E. A. Williams, T. Boehly, R. L. Keck, K. Tanaka, and R. Boni, "Nonlinear Interaction Mechanisms in UV-Laser Plasmas," presented at the Twelfth Annual Conference on Anomalous Absorption of Electromagnetic Waves, Sante Fe, New Mexico, May 1982.

R. W. Short and E. A. Williams, "Frequency-Broadening Arising from Filamentation in a Laser-Plasma Corona," presented at the Twelfth Annual Conference on Anomalous Absorption of Electromagnetic Waves, Sante Fe, New Mexico, May 1982.

S. Skupsky and K. Lee, "Uniformity of Illumination and Thermal Smoothing for Laser-Driven Fusion," presented at the Twelfth Annual Conference on Anomalous Absorption of Electromagnetic Waves, Sante Fe, New Mexico, May 1982.

E. A. Williams and R. W. Short, "Stimulated Brillouin Scattering of Multi-Line Laser Light in a Flowing Plasma Corona," presented at the Twelfth Annual Conference on Anomalous Absorption of Electromagnetic Waves, Sante Fe, New Mexico, May 1982.

J. Delettrez, B. Yaakobi, M. C. Richardson, T. Boehly, R. S. Marjoribanks, S. Letzring, R. Hutchison, R. McCrory, and J. Soures, "Energy Transport and Partitioning in Nanosecond One-Micron Spherical Target Irradiation Experiments," presented at the 1982 IEEE International Conference on Plasma Science, Ottawa, Ontario, Canada, May 1982.

S. Kacenjar, L. M. Goldman, S. Skupsky, A. Entenberg, M. C. Richardson, and J. M. Soures, "Direct Measurement of Core Density-Radius Product of Laser Fusion Targets," presented at 1982 IEEE International Conference on Plasma Science, Ottawa, Ontario, Canada, May 1982.

R. S. Marjoribanks, M. C. Richardson, S. A. Letzring, and J. Delettrez, "Time-Resolved X-Ray Spectroscopy of OMEGA Laser-Driven Symmetric Compressions," presented at the 1982 IEEE International Conference on Plasma Science, Ottawa, Ontario, Canada, May 1982.

M. C. Richardson, D. M. Villeneuve, B. Yaakobi, J. Delettrez, S. Skupsky, W. Friedman, J. Hoose, S. Letzring, J. Rizzo, R. L. McCrory, and J. M. Soures, "Twenty-Four Beam Nanosecond Irradiation Experiments with Spherical Targets," presented at the 1982 IEEE International Conference on Plasma Science, Ottawa, Ontario, Canada, May 1982.

W. Seka, "UV-Laser Matter Interaction Processes," presented at the 1982 IEEE International Conference on Plasma Science, Ottawa, Ontario, Canada, May 1982.

R. Leary, "Managing Size and Complexity in Large FORTH Applications," presented at the 1982 Rochester FORTH Conference, Rochester, New York, May 1982.

S. Zoeller, T. Sizer, and J. Kafka, "Measurement of Amplified Femtosecond Pulses," presented at the 1982 Rochester FORTH Conference, Rochester, New York, May 1982.

M. C. Richardson, "Recent Progress in the Direct-Drive Approach to Laser Fusion," invited paper presented at the Annual Meeting of the Plasma Physics Division, Oxford, England, June 1982.

T. M. Nordlund, "Subnanosecond Fluorescence Measurements of Tryptophan and Tyrosine Motions," presented at the Tenth Annual American Society for Photobiology, Vancouver, B.C., June 1982.

J. D. Kafka, T. Sizer II, C. W. Gabel, and G. Mourou, "Synchronous Amplification of Seventy Femtosecond Pulses Using a Frequency-Doubled Nd:YAG Pumping Source," presented at the Third Topical Meeting on Picosecond Phenomena III, Garmisch-Partenkirchen, Federal Republic of Germany, June 1982.

W. Knox, T. M. Nordlund, and G. Mourou, "Jitter-Free Streak Camera System," presented at the Third Topical Meeting on Picosecond Phenomena III, Garmisch-Partenkirchen, Federal Republic of Germany, June 1982.

S. Williamson and G. Mourou, "Electron Diffraction in the Picosecond Domain," invited talk at the Third Topical Meeting on Picosecond Phenomena III, Garmisch-Partenkirchen, Federal Republic of Germany, June 1982.

J. Kafka, T. Sizer II, I. N. Duling, C. W. Gabel, and G. Mourou, "Synchronous Amplification of 70 Femtosecond Pulses Using a Frequency-Doubled Nd:YAG Pumping Source," invited talk at the Third Topical Meeting on Picosecond Phenomena III, Garmisch-Partenkirchen, Federal Republic of Germany, June 1982.

T. E. Orlowski, B. A. Weinstein, W. H. Knox, T. M. Nordlund, and G. Mourou, "Picosecond Radiative and Non-Radiative Recombination in Amorphous AS_2S_3," presented at the Third Topical Meeting on Picosecond Phenomena III, Garmisch-Partenkirchen, Federal Republic of Germany, June 1982.

W. Knox, G. Mourou, and T. M. Nordlund, "Application of Jitter-Free Streak Camera in Solid State Physics, Biophysics and Chemistry," presented at the Twelfth International Quantum Electronics Conference, Munich, Germany, June 1982.

G. R. Baker, D. I. Meiron, S. A. Orszag, R. L. McCrory, and C. P. Verdon, "Iterative Boundary Integral Methods for Free Surface Flow Problems in Two and Three Dimension," invited talk at the Twelfth International Quantum Electronics Conference, Munich, Germany, June 1982.

T. Sizer II, J. D. Kafka, I. N. Duling, C. W. Gabel, and G. Mourou, "Generation and Amplification of 70 Femtosecond Pulses Using a Frequency-Doubled Nd:YAG Pumping Source," presented at the Twelfth International Quantum Electronics Conference, Munich, Germany, June 1982.

S. Williamson and G. Mourou, "Electron Diffraction in the Picosecond Domain," invited talk at the Twelfth International Quantum Electronics Conference, Munich, Germany, June 1982.